Thin–Walled Structures 192 (2023) 111128

Contents lists available at ScienceDirect

Thin-Walled Structures

journal homepage: www.elsevier.com/locate/tws

Review

State-of-the-art review on the web crippling of pultruded GFRP profiles

Chao Wu [a,*], Yue Ding [b], Lourenço Almeida-Fernandes [c], José Gonilha [c,e], Nuno Silvestre [d], João R. Correia [c,*]

[a] Department of Civil and Environmental Engineering, Imperial College London, South Kensington Campus, London, UK
[b] School of Transportation Science and Engineering, Beihang University, 37 Xueyuan Road, Beijing 100191, China
[c] CERIS, Instituto Superior Técnico, University of Lisbon, Portugal
[d] IDMEC, Instituto Superior Técnico, University of Lisbon, Portugal
[e] Instituto Superior de Educação e Ciências (ISEC Lisboa), Alameda das Linhas de Torres, 174, 1750-142 Lisboa, Portugal

ARTICLE INFO

Keywords:
Web crippling
Local failure
Transverse loading
Fibre reinforced polymer
Composites
Pultruded profiles
Review

ABSTRACT

Web crippling involves the failure of pultruded glass fibre reinforced polymer (GFRP) profiles under transverse concentrated loading. The possible failure modes include web buckling, web crushing and web-flange junction failure, which are very different from those of metallic sections, which are isotropic and yield. This paper provides a comprehensive review of the up-to-date research advancement in web crippling of pultruded GFRP profiles from four perspectives. Firstly, the experimental results available in the literature are summarized and a database is tabulated. Secondly, the factors influencing failure modes and web crippling resistance are analysed, including loading conditions, section geometries, and material properties. Thirdly, recent advancement in numerical modelling is reviewed and paths for improvement are identified. Lastly, analytical models for predicting web crippling resistance are reviewed and their accuracy is assessed by comparing predictions with experimental results from the database. It is concluded that this research area is still in its early stages and more experiments need to be conducted, in a standardized and systematic manner; in addition, more detailed material properties should be characterized for a better interpretation of the failure mechanisms. Accurate and reliable analytical models covering all design cases are not yet available, and most existing analytical models still need to be validated with independent experimental data. Finally, the paper identifies key research gaps and proposes future research directions. This paper also provides a benchmark for the future development of design provisions regarding the web crippling of pultruded GFRP profiles.

1. Introduction

In the past few decades, pultruded glass fibre reinforced polymer (GFRP) sections have been increasingly used in civil engineering structural applications [1,2]. GFRP profiles have important advantages in construction, such as high strength, light weight, corrosion resistance, convenient installation, and electromagnetic transparency [3]. However, due to the specificities of the manufacturing process, the fibres are mainly aligned in the pultrusion direction (the axial direction of the member), while much less fibre reinforcement is used in the transverse direction, leading to a high orthotropy of pultruded members, i.e. the mechanical properties along the transverse direction are much lower than those in the axial direction.

In structural applications, it is difficult to avoid the introduction of transverse stresses to profile members, owing to transverse concentrated loads (e.g. reaction forces at beam ends, coupling forces at beam-to-column connections). In these cases, premature web crippling failure of pultruded GFRP profiles may occur, limiting the exploitation of the superior axial mechanical properties of the profiles. In addition, existing design guidelines for pultruded FRP structures, such as the Eurocomp Design Code [4], the Italian Guidelines [5] and the European Technical Specification (CEN/TS 19101) [6], do not provide design clauses that specifically address web crippling. Only the ASCE pre-standard [7] includes design formulae for predicting the resistance to web crippling. However, that formulae, based on the research of Borowicz and Bank [8], were calibrated only for interior-one-flange (IOF) and end-one-flange (EOF) configurations. Another two common transverse loading conditions are end-two-flange (ETF) and interior-two-flange (ITF) [9], which are not covered by the ASCE pre-standard. In addition, some researchers have also considered end-ground (EG) and

* Corresponding authors.
E-mail addresses: c.wu@imperial.ac.uk (C. Wu), joao.ramoa.correia@tecnico.ulisboa.pt (J.R. Correia).

https://doi.org/10.1016/j.tws.2023.111128
Received 15 February 2023; Received in revised form 16 August 2023; Accepted 17 August 2023
Available online 28 August 2023
0263-8231/© 2023 The Author(s). Published by Elsevier Ltd. This is an open access article under the CC BY-NC-ND license (http://creativecommons.org/licenses/by-nc-nd/4.0/).

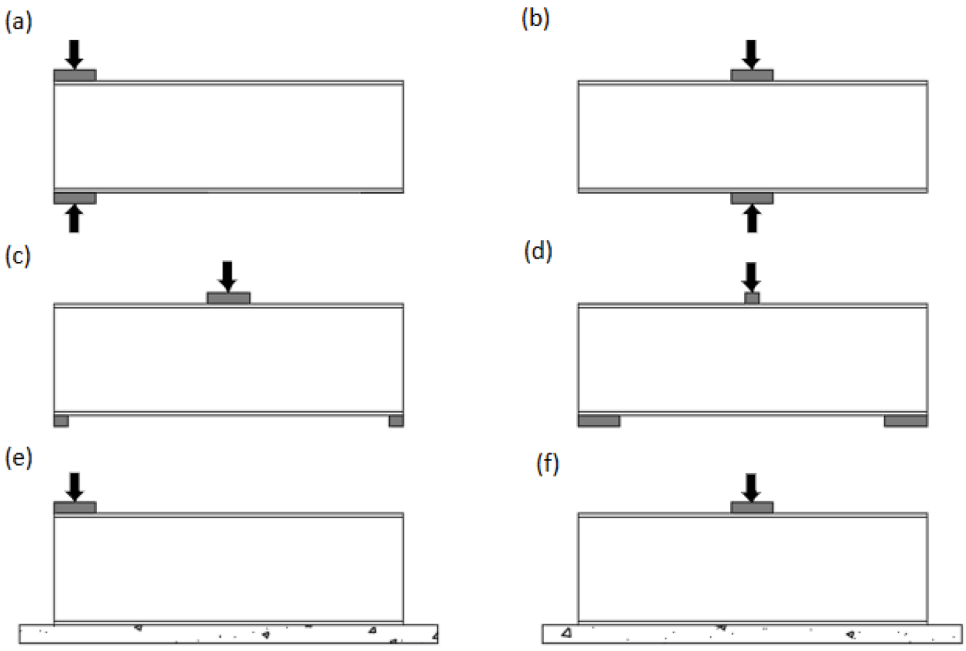


Fig. 1. Definition of web crippling loading conditions: (a) ETF; (b) ITF; (c) EOF; (d) IOF; (e) EG; (f) IG.

interior-ground (IG) conditions, where specimens are placed on the ground and are subjected to an end or interior bearing load, respectively, on the opposite flange [10]. These two conditions are less common in practice and may correspond to applications in foundations when the sections are laid on the ground with loading applied on the top flanges. These loading conditions are shown in Fig. 1.

Web crippling is a general term describing the failure behaviour of thin-walled sections when subjected to transverse loading conditions, as those in Fig. 1. It was first investigated in metallic thin-walled sections [11,12], including cold-formed steel sections [13,14] and aluminium sections [15,16]. For metallic sections, web crippling refers to web yielding or web buckling failure [17]. For pultruded GFRP profiles, on the other hand, web crippling occurs with different and more complex failure modes, i.e. web-flange junction failure, web crushing and/or web buckling [18], which are discussed in the following sections. The web crippling behaviour is fundamentally different between steel and pultruded GFRP sections in that (1) steel is ductile while GFRP is brittle, and (2) steel is isotropic, while GFRP is orthotropic.

This paper presents a state-of-the-art review on the web crippling behaviour of pultruded GFRP profiles, presenting (i) a review and a database of experimental tests, (ii) numerical simulations, and (iii) analytical models for the prediction of web crippling capacity. The predictions from these theoretical models are compared with the experimental results from the literature, and their accuracy is assessed. This review aims to provide an experimental and theoretical basis for the future development of design guidance concerning the web crippling of pultruded GFRP profiles.

2. Experimental studies

2.1. Summary of previous studies

Web crippling has been extensively studied for metallic sections, for which extensive experimental and theoretical results are available in the literature. However, research programmes specifically designed to understand the web crippling behaviour of pultruded GFRP profiles did not exist until the 2010s. This section reviews the experimental studies on the web crippling behaviour of pultruded GFRP profiles developed since then.

Borowicz and Bank [8] investigated the flexural behaviour of pultruded GFRP I-shaped beams subjected to three-point bending. Twenty beams, with a nominal height ranging from 152.4 mm to 304.8 mm, were tested with a span-to-height ratio of 4. The load was applied to the top flange with or without a bearing plate of varying width and thickness. All test specimens failed with a wedge-like shear failure at the upper web-flange junction. It was also found that the beam capacity could be increased when the bearing plate had greater length and thickness.

Wu and Bai [18] reported a pioneer investigation on the web crippling behaviour of pultruded GFRP rectangular hollow sections (RHS) under four loading conditions: ETF, ITF, EG, and IG. The authors aimed to highlight the significant differences between the web crippling behaviour of pultruded GFRP profiles and that of metallic sections. The GFRP profiles failed due to web buckling failure or web-flange junction failure, both of which were brittle and the latter was never observed in metallic sections. They also proposed an analytical model (described in section 4.2) based on the web-flange junction failure mechanism and the predictions agreed well with the experimental results.

After these two early studies, more researchers started extensive investigations and significantly contributed to a better understanding of the web crippling behaviour of pultruded GFRP profiles. Chen and Wang carried out experiments on a pultruded GFRP RHS [19] and a I-shape section [20] under four loading conditions: ITF, ETF, IG and EG, each with three different bearing lengths of 50 mm, 100 mm and 150 mm. Web buckling in the RHS section and web shear failure in the I-section were observed after initial cracking at the web-flange junction. The same research group also conducted web crippling testing of a pultruded GFRP channel section [21], with the same loading conditions and bearing lengths adopted in the tests of the RHS and I-shaped sections. Web buckling was the main failure mode and similar design formulae were proposed for the four loading conditions.

The CORE Group at the University of Lisbon has conducted extensive investigations on the web crippling of pultruded GFRP profiles. Almeida-Fernandes et al. [22] reported an experimental study on the web-crippling of GFRP pultruded I-shaped sections with a nominal height ranging from 100 mm to 400 mm. Two loading conditions of ETF and ITF were adopted, each with three different bearing lengths of 15 mm, 50 mm, and 100 mm. Web-flange junction failure, web crushing in

the centre of the web, and web buckling were observed. The effect of loading condition and bearing length on the bearing capacity and stiffness were quantified and discussed.

This research group [23] reported another study on the web crippling of I-shaped and channel sections under ETF and ITF conditions. Four I-shaped sections and one channel section from different suppliers were tested with three bearing lengths. The failure modes were assessed through strain gages and a video-extensometer, to monitor the side view of the specimens. In addition, the in-plane strains were monitored to assess the effect of fibre layup and bearing length on the shear and transverse compressive stresses of the web. Web-flange junction failure, web buckling failure or a combination thereof were observed.

Haloi et al. [24] investigated the web-crippling behaviour of pultruded GFRP wide flange I-sections under ETF and ITF conditions. Five bearing lengths ranging from 25 mm to 125 mm and two bearing thicknesses of 8 mm and 10 mm were adopted for the tests. Most of the specimens failed due to web-flange junction separation followed by web crushing. No specimen showed out-of-plane web deformations or web buckling. It was found that the bearing length influenced the bearing capacity, while the bearing thickness showed little effect on strength.

Estep et al. [25] conducted three-point bending tests on pultruded GFRP RHS beams. The beams exhibited three different failure modes depending on the span-to-height ratio (L/H). For short span beams, local buckling failure of the compression flange and localized web crushing at the loading point were observed. For intermediate spans, longitudinal tensile failure occurred in the web, while for long span beams, longitudinal tensile failure was observed in the flange. It was obvious that the short span beams experienced premature local failure due to web crippling under IOF loading condition. Design formulae were proposed, but they were used to predict the global flexural capacity of the beam rather than the local web crippling resistance.

Oskouei et al. [26] studied the effect of wet-dry cycles, under different sea water conditions, on the flexural and web crippling behaviour of a pultruded GFRP I-shaped section. The IOF loading condition was adopted for the web crippling tests. The I-shaped section was stocky, therefore no stability issues were observed. Specimens failed due to web crushing close to the web-flange junction, regardless of the ageing process. A maximum reduction of about 10% in load carrying capacity was observed due to material degradation.

Gand et al. [27] presented an experimental programme to investigate the effect of web perforations on the web crippling behaviour of a pultruded GFRP I-shaped section with 152 mm of height. The web was perforated with either a circular or a rectangular opening, corresponding to ~19% and ~18% of the total web area. The sections were subjected to four loading conditions, including ITF, ETF, IG and EG. It was found that the web-flange junction cracking was the dominant failure mode for all sections regardless of web opening. Cracking in the web at the corner of the rectangular opening was also observed for some specimens. The results showed that the section capacity reduced by 20% with a circular opening and 25% with a rectangular opening.

Singh and Chawla [28] carried out tests in pultruded FRP I-section beams under IOF and EOF loading conditions. A total of eight specimens were tested, including two types of fibre architecture and two different bearing lengths (40 mm, 125 mm). The failure mode of all specimens was web crushing and the bearing length and fibre architecture were reported to influence the ultimate bearing capacity of the specimens.

Wu et al. [10,29,30] reported a study on the web crippling behaviour of four pultruded GFRP channel sections with different dimensions under ETF and ITF loading conditions. The effect of bearing length was also investigated. The web crippling capacities increased by 367% (ITF) and 567% (ETF) when the bearing plate length changed from 20 mm to 200 mm [30]. Web bucking and web-flange junction cracking were observed depending on the web slenderness, bearing length and loading condition.

The previous studies show that the web crippling of pultruded GFRP profile is a complex phenomenon, which can be influenced by many factors, including section shape and dimensions, material properties, bearing length and loading conditions. These factors, which may affect the web crippling with respect to the failure mode, load-displacement response and bearing capacity, are discussed in further depth in the next subsections.

2.2. Factors influencing the web crippling behaviour

Besides the loading conditions, previous studies have shown that the web crippling phenomenon is influenced by (i) geometrical factors, namely the shape and dimensions of the cross-section, and (ii) material properties, such as the elastic moduli and strengths (e.g. the interlaminar shear strength at the web flange junction, and the in-plane shear and transverse compressive strengths of the web) of the GFRP pultruded section.

Regarding the section shape, previous studies have focused mostly on RHS, I-shaped section and channel section profiles. RHS and I-shaped section are double symmetric sections, which are the most likely to be subjected to significant transverse concentrated loading in structural applications. Channel sections are single symmetric and almost all studies on channel sections applied transverse loading on the flanges. All the specimens (a total of 199) from the published literature on the web crippling behaviour of pultruded GFRP profiles are collected and listed in Table S1 (supplementary material). Their section shapes and dimensions are summarized in Table 1, together with the web slenderness. The discussions in this paper are based on the experimental results of GFRP profiles with dimensions listed in Table 1. Another relevant geometrical parameter, important in the web crippling design of metallic sections, is the interior corner radius at the web-flange junction. However, most of the studies on pultruded GFRP profiles have neglected (or did not report) this parameter. When available, this parameter has been included in Table S1. It is recommended that future studies include the measurement of this radius and evaluate its effect, allowing to include this parameter in the development of new design models.

Regarding the material properties of pultruded GFRP profiles, the elastic moduli and strength reported in the literature are listed in Table S2 and summarized in Table 2. Table 2 aims to summarize the material properties of GFRP sections that have been tested in the literature (see Table S2). Because researchers used different GFRP sections (provided by different manufacturers) for web crippling testing, the material properties vary in a wide range. This table quantifies the scope of the discussions in this review, i.e. the statements and findings are only applicable to GFRP sections with the properties reported in Table 2. The tensile strength and modulus in the pultrusion direction are the most often reported properties, even though under web crippling testing the load is applied in the transverse direction. However, very few studies reported the compressive properties of the web in the transverse direction, possibly due to the limited height of the webs of typical pultruded profiles, making it difficult to retrieve specimens for standard compression strength testing. However, typical web crippling failure modes, such as web buckling or web crushing, are dependent on the transverse compressive strength and elastic modulus of the material.

Table 1
Section shapes and range of sectional dimensions in the web crippling studies.

Section shape	Section height, H (mm)	Section width, W (mm)	Flange thickness, t_f (mm)	Web thickness, t_w (mm)	Web slenderness *
RHS	50 to 102	50 to 102	4.0 to 10.2	4.0 to 10.2	14.1–77.7
I-shaped	99 to 400	50 to 200	5.6 to 15.0	5.8 to 15.0	38.9–83.0
Channel	99 to 203	29 to 56	4.7 to 6.4	4.8 to 6.4	48.3–102.9

* The standard definition for the slenderness of cross-section wall elements is the width-to-thickness ratio. In Wu et al. [10], an alternative definition was used: the web height divided by the radius of gyration of the web with respect to its midline (see Eq. (4n) and Eq. (4q) in section 4.2). In this paper, the latter definition is adopted.

Table 2
Mechanical properties of pultruded GFRP profiles in the web crippling studies.

Section shape	Longitudinal Tensile strength, $f_{L,t}$ (MPa)	Tensile modulus, $E_{L,t}$ (GPa)	Transverse Compressive strength, $f_{T,c}$ (MPa)	Compressive modulus, $E_{T,c}$ (GPa)	In-plane shear Strength, f_{LT} (MPa)	Modulus, G_{LT} (GPa)	Interlaminar shear strength, f_s* (MPa)
RHS	275–283	25–26	NA*	NA	NA	NA	28–29
I-shaped	240–425	22.8–44.0	46–123	1.8–10.9	19.9–46.8	3.0–4.1	25.0–38.3
Channel	269–376	25.0–25.2	56.5	8.6–13.0	NA	NA	27.8–33.8

* Interlaminar shear strength can be evaluated using either off-axis tensile testing or short-beam testing. NA refers to 'not available'. More details can be found in Table S2 in the supplementary material.

Without experimentally characterizing those properties, the mechanical analysis of these phenomena is not possible.

As for the shear properties, because pultruded GFRP profiles are highly orthotropic, there are two relevant shear behaviours: (i) in-plane shear and (ii) interlaminar shear, both illustrated qualitatively in Fig. 2. The interlaminar shear occurs in a plane that is parallel to the planes between the plies of the laminate, while for in-plane shear (which can be translaminar or intralaminar) the crack plane is orientated transversely to the ply plane. Normally the in-plane shear strength can be determined using the sample shown in Fig. 2, while the interlaminar shear strength is obtained from three-point bending tests on short beam specimens. A simplified method to determine the in-plane shear property was proposed by *Nguyen* et al. [31] using 10° off-axis tensile test but this method has not been standardized yet. The shear strength was less often reported in the literature. In previous web crippling studies, cracking at the web-flange junction has been frequently observed. The web-flange junction is subjected to complex stress states, consisting of compression in the transverse and/or in the longitudinal directions (in case of IOF), and interlaminar shear. Furthermore, the web-flange junction of pultruded profiles is a resin rich zone having different fibre architecture and fibre content compared with the web and flange. Therefore, it is recommended that future studies experimentally characterize the compressive properties of the web in the transverse direction and the in-plane and interlaminar shear strengths. The development of new technologies and testing techniques to characterize the complex stress state and constitutive models of pultruded material at the web-flange junction is also encouraged.

2.3. Failure modes

Three failure modes have been frequently reported in previous web crippling studies of pultruded GFRP profiles: web crushing, web buckling, and web-flange junction failure (cracking or separation at the web-flange junction). In this review, web crushing is defined as a material strength failure under compression in the plane of the web. Web crushing can (i) occur at mid-height of the web with cracking extending in the longitudinal direction (Fig. 3a), or (ii) it can be localised at the web-flange junction, immediately underneath the loading point (Fig. 3b). The crushing may result in a shear like crack in the web (Fig. 3c, this occurs due to exceeding material interlaminar shear strength) or a compression like crack (Fig. 3d, this occurs due to exceeding material compression strength). Shear like cracks are much easier to recognise, while compression like cracks have a similar pattern to buckling induced cracks (Fig. 4). In this case, the out-of-plane deformation (Fig. 4) should be monitored to confirm whether the crack is due to crushing or buckling.

Web buckling failure is defined as an instability failure of sections with a slender web. It is normally informed by an out-of-plane deformation of the web (Fig. 4). Ultimate failure is triggered by web cracking in the longitudinal direction due to extensive buckling deformation, as shown in Fig. 4. The web recovers the out-of-plane deformation after the load is removed, so, as mentioned earlier, the cracking due to buckling can be confused with that due to crushing, especially when the out-of-plane deformation is not monitored during loading (or is limited).

Web-flange junction failure normally involves a localised cracking, which develops underneath the bearing load. Normally the crack initiates at the web-flange junction and propagates in the longitudinal direction, leading to the separation between the web and flange (Fig. 5a, this occurs due to exceeding interlaminar shear strength at the junction). Most of the time, an inclined crack for RHS and channel sections (Fig. 5b) or a wedge like crack for I-shaped sections (Fig. 5c) is observed at the web-flange junction. After web-flange junction failure, the load is transferred to the web and sometimes local web crushing can also be observed (Fig. 3b). Please note that Figs. 3 to 5 use a channel section to demonstrate the typical failure modes that pultruded sections may have. These failure modes are not exclusive to channel sections and may occur in different section shapes.

In most experimental programs, a combination of the three types of failure modes is more often reported, and it can be difficult to distinguish their occurring sequence. Therefore, it is important to develop experimental techniques to monitor the occurring sequence of the different failure modes, adopting comprehensive and tailored instrumentation to capture the relevant deformations. This will be essential to develop mechanism-based analytical models to predict the web crippling capacity of pultruded GFRP profiles.

2.4. Load vs. displacement response

The typical load vs. displacement response of pultruded GFRP profiles under web crippling loading can be described by two general stages, as shown in Fig. 6. The linear ascending branch of the curve before the peak point is the first stage and the rest of the curve is the second stage. The peak point is denoted with a dash line. The two-stage pattern is independent of the section shape, material properties, bearing length and loading conditions. In the first stage, the load increases linearly with the displacement up to a peak point and then drops suddenly due to either web crushing, web buckling or web-flange junction failure. Normally, the load drops to a lower level and then the second stage starts. Load fluctuation is generally observed in the second stage, namely due to progressive failure in the web. The fluctuations do not usually surpass the initial peak load, although this can occasionally occur, indicating that the progressive failure mechanism may generate higher resistance.

2.5. Web crippling capacities

It is recommended that the load at the first peak point of the load vs. displacement curve be taken as the web crippling capacity, even though the load in the second stage may be higher. This is because the first peak load normally corresponds to one of the three typical failure modes, when the section has already lost its integrity.

Tables S3, S4 and S5 summarize the web crippling capacities of all specimens tested in the literature, with respect to different loading conditions, in particular, Table S3 for ETF and ITF conditions, Table S4 for EOF and IOF conditions, and Table S5 for EG and IG conditions. These tables report tests of 75 specimens under ETF, 76 specimens under ITF, 11 specimens under EOF, 13 specimens under IOF, and 12 specimens under EGF and IGF.

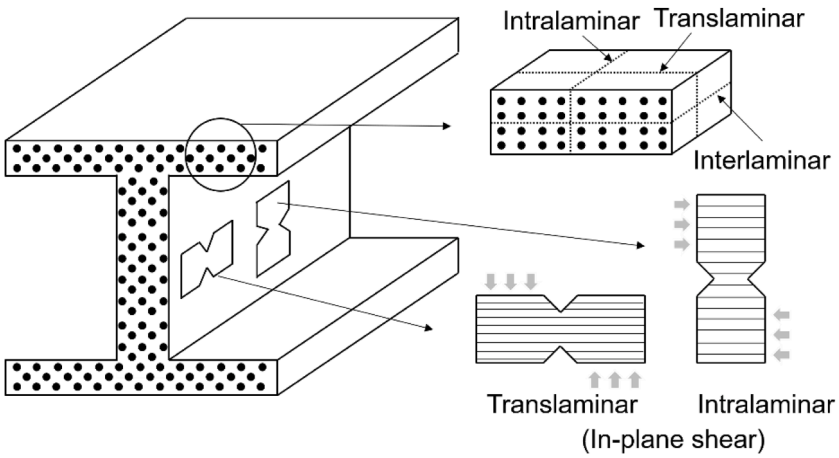


Fig. 2. Definition of in-plane and interlaminar shear stresses of pultruded GFRP profiles.

Figs. 7-10 assess the influence of several parameters – cross-section shape, web transverse crushing resistance and flexural stiffness, and bearing length – on the web crippling capacity. Because the objective of these figures is only to provide a qualitative assessment of the influence of these parameters on the resistance to web crippling, such capacity is divided by the thickness and height of the web(s).[1]

Fig. 7 presents the effect of section shape on the failure mode and web crippling bearing capacity under different loading conditions. All data points for RHS are marked in black, those for I sections are in red and data for channel sections are in green. For the same section shape, the failure modes are marked with different bullet shapes, i.e. circle for web buckling, triangle for web crushing and star for web-flange junction failure (WFJ).

In terms of failure modes, theoretically, they should not be directly associated with the section shape. In other words, for the same section shape, it is possible to observe all three failure modes under any loading conditions. If any failure mode is not observed for a given section shape, this means that more testing for that section shape with different dimensions is needed. For example, as shown in Fig. 7, web crushing was not observed for channel sections. This does not mean that channel sections will never experience web crushing failure. This just indicates that the results of tests of channel sections are limited in the literature and more testing is needed.

In Fig. 7, it seems that channel sections exhibit relatively lower capacity (e.g. 30 to 125 MPa under ITF condition) than the RHS and I-shaped sections with a capacity ranging from 50 to 250 MPa. This might be because channel sections are asymmetric and tend to fail due to buckling comparing with symmetric sections like RHS and I-shaped with the same web area.

The effect of web properties on the failure mode and web crippling capacity is presented in Fig. 8 and Fig. 9 under different loading conditions. The web properties are associated with respectively web crushing (Fig. 8) and web buckling (Fig. 9) resistances. The horizontal axis in Fig. 8 is presented as the theoretical web crushing capacity per unit web length, which is given by the web transverse compressive strength $f_{T,c}$ times the thickness of the web t_w. The web transverse compressive strength is used because it is one of the most relevant material properties under transverse bearing load.

In terms of failure modes, it is clearly observed that with the increase in $f_{T,c} \times t_w$, web crushing becomes a dominant failure mode. However, there is no clear trend in the web crippling capacity per unit web area when $f_{T,c} \times t_w$ increases. In other words, increasing the theoretical web crushing capacity per unit web length ($f_{T,c} \times t_w$) does not necessary provide greater web crippling capacity of the section that is generated by a unit area of the web.

The effect of web transverse flexural stiffness on the failure mode and web crippling capacity is presented in Fig. 9 under different loading conditions. The web transverse flexural stiffness is given as the web transverse compressive modulus $E_{T,c}$ times the ratio between the cube of the web thickness t_w and the web height h_w. This is an indicator of the theoretical web buckling capacity under the transverse bearing load.

In terms of failure modes, it seems that the WFJ failure becomes dominant when the web has a greater flexural stiffness. It is difficult to distinguish web buckling and web crushing failure when the web transverse flexural stiffness is relatively low. Again, no clear trend was observed for the web crippling capacity per unit web area as a function of the web transverse flexural stiffness. Note that in steel sections it is possible to establish a dimensional limit to avoid web buckling failure, namely by controlling the web slenderness ratio. This is because steel has a well-defined modulus of elasticity (i.e. not dependent on the manufacturer or cross-section). On the other hand, establishing such a geometric limit is not possible for pultruded GFRP sections, since different profiles in general present different web moduli.

The effect of bearing length on the failure mode and web crippling capacity is presented in Fig. 10 for different loading conditions. For each loading condition, the horizontal axis represents the bearing length in mm. It is assumed that the bearing plate is much more rigid than the pultruded GFRP profile and the bearing plate covers the whole width of the flange. This means that the thickness and width of the bearing plate have little effect on the web crippling behaviour and only the bearing length is relevant.

In terms of failure modes, under the same loading condition, with the increase of bearing length they tend to change from web crushing to web buckling or WFJ. This is because for shorter bearing lengths stress concentrations are higher, leading to localized material failure under the bearing plates. It is also observed that, under the same loading condition, the web crippling capacity per unit web area increases with the increase of bearing length. This may be because with longer bearing length, more material in the section is engaged in load carrying; in other words, the load is more uniformly distributed along the length of the web. Again, these trends are obvious for ETF and ITF loading conditions. For the other loading conditions, owing to the limited experimental data available, no clear trends can be found.

[1] Regarding the web crippling resistance mechanisms (discussed in further depth in section 4), it is known that the applied load spreads from the bearing plates to the web and the stresses propagate along the web height. Since these stresses also vary along the beam length, a general and accurate definition of the area where the stresses trigger crippling does not exist. Usually, an accepted approach to define the web area resisting to web crippling is to adopt an effective length, B_{eff}, multiplied by the web thickness, t_w. Therefore, in Figs. 7 to 10, a simplifying assumption is made that $B_{eff} = h_w$ for all situations considered.

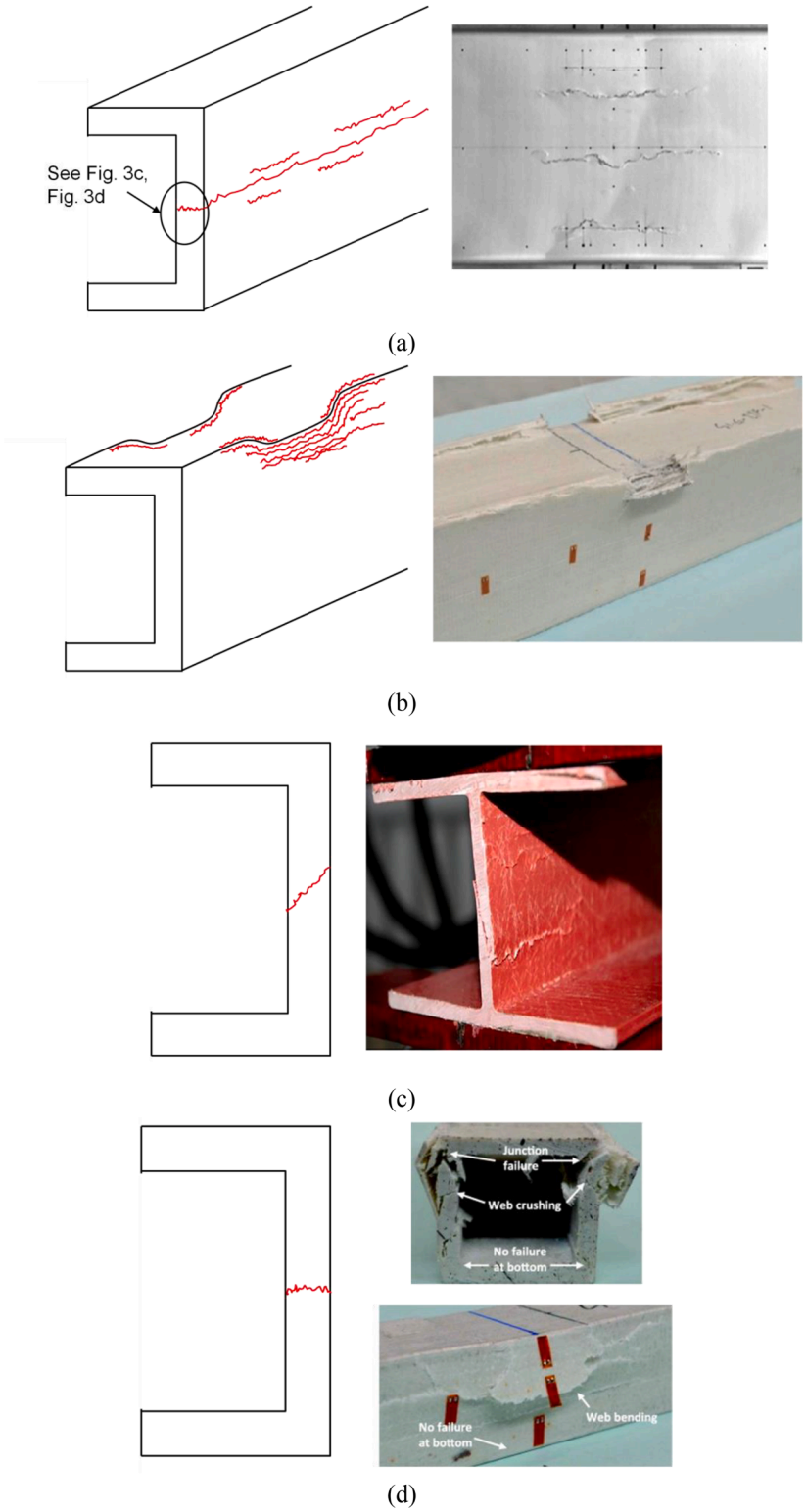


Fig. 3. Typical web crushing failure modes: (a) web crushing at mid-height of the web, photo from [23]; (b) web crushing under the loading point, photo from [18]; (c) web crushing with a shear like crack, photo from [24]; (d) web crushing with a compression like crack, photo from [18].

3. Numerical studies

Although some experimental results on web-crippling of FRP profiles have been reported, few authors have attempted to numerically simulate those tests. Such an absence of numerical studies may be explained by the following reasons:

1. The failure of FRP materials is brittle, and the failure and damage progression criteria currently available (by default) in commercial FE packages still have some limitations (*e.g.* the widely known Hashin criterion was developed for unidirectional composites [32], hindering its application to multi-directional stress states in pultruded composites).

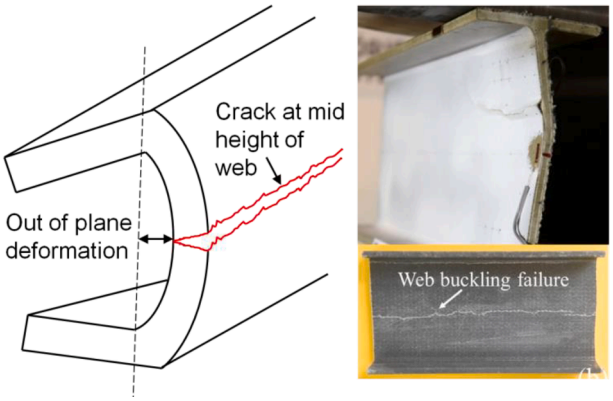


Fig. 4. Typical web buckling failure mode with a crack at the mid height of the web due to its out-of-plane deformation, photos from [10,23].

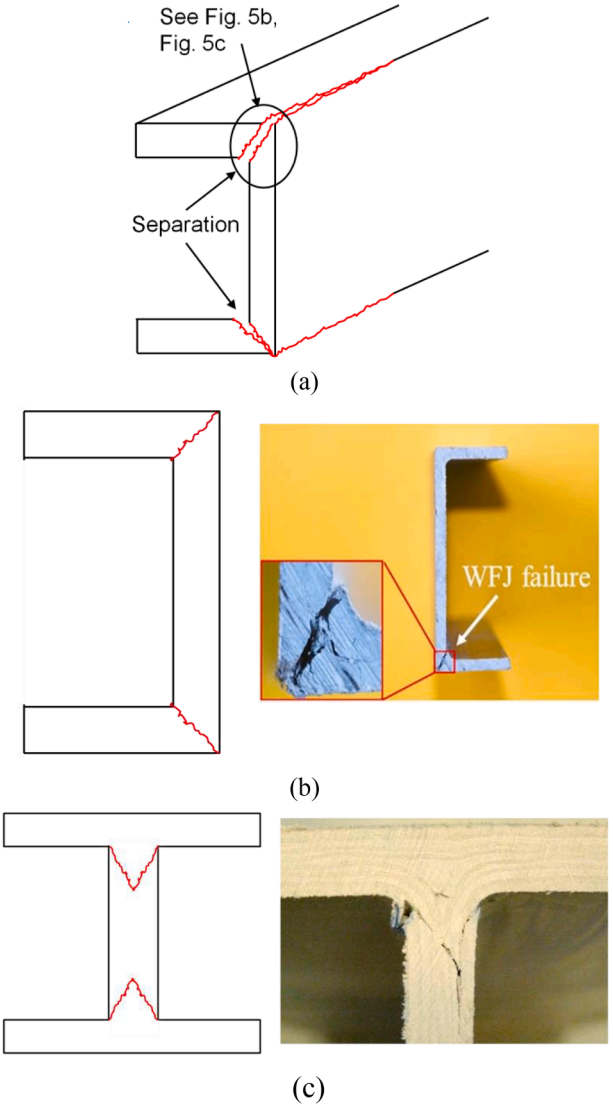


Fig. 5. (a) Typical web-flange junction failure with (b) an inclined cracking for RHS or channel section, photo from [10] or (c) a wedge like cracking for I-shaped section photo from [8].

2. The fracture energy of FRPs is a mechanical property that has been neglected in the characterization of these materials for many years. Because some failure and damage progression criteria require this knowledge, the users of commercial FE packages either adopt values they found in the literature for other dissimilar materials or simply stop the modelling procedure due to lack of data on fracture energy.
3. The web crippling failure often arises from transverse compressive loading. The failure and damage progression criteria gets more complex in compression than in tension, due to the cohesion between the two contacting cracked surfaces, a phenomenon that is extremely difficult to simulate. Usually this is done by including compressive residual stress in the damage progression criterion [33,34].
4. The bearing plates tend to cause local damage to the beam flanges in their edges and the crippling failure mode turns very localised in the web, setting this problem into a complex three-dimensional phenomenon. The localization of damage always requires a very refined FE mesh to accurately simulate the stress/strain concentration, and it is well known that the convergence of results strongly depends on the balance between the FE mesh and composite material failure criterion.
5. The inherent complexity of analysing the geometrical and mechanical properties of the matrix-rich web-flange zone [35,36] has also hampered accurate simulations of web-crippling phenomena.

In summary, the factors listed before are still hindering a more extensive application of numerical FE methods to analyse web crippling failure of pultruded FRP profiles. Despite this evidence, some relevant numerical studies were carried out and they are described below by chronological sequence.

In 2011, Borowicz and Bank [8] used finite element (FE) modelling to simulate a web-crippling test of pultruded profiles (SW-W8-VE, *cf.* Table S1), with the limited objective of analysing the stress and strain state at the web-flange junction. The authors carried out linear elastic analysis, with the commercial software ANSYS 11.0 [37] using solid elements (SOLID 185) to model all elements and 3D contact elements (details of which were not provided). The steel roller which applied the displacement to the GFRP profile was modelled as isotropic, while all GFRP laminates involved, i.e. bearing plates, web and flanges, were modelled as orthotropic. In this regard, it should be mentioned that the elastic properties considered as input were representative properties of pultruded GFRP profiles taken from previous experimental tests (on different GFRP profiles). The numerical results supported the experimental observations in terms of strain gauge readings and digital image correlation (DIC) data.

Almeida-Fernandes et al. [22] presented a FE modelling of an extensive experimental campaign [9], *cf.* Table S1, which included 4 different GFRP profiles, 3 bearing lengths and 2 load configurations (ETF and ITF). With the commercial package ABAQUS [38], the authors used 4-node shell elements with reduced integration (S4R) to model the GFRP laminates (web and flanges) and 8-node solid elements with reduced integration (C3D8R) to model the steel bearing plates. The GFRP laminates were modelled with their nominal thickness without considering the web-flange junction fillet radius, i.e. the connection between web and flanges was made at a 90° angle. The GFRP web and flanges were modelled as orthotropic, using the elastic properties obtained from experimental material characterization tests [9] for each section wall, while the steel material was modelled as isotropic. All materials were modelled as linear elastic. Load was applied to the GFRP profiles by imposing a downward load on the top bearing plate, while the bottom bearing plate was fixed (as in the tests). The interaction between the GFRP flanges and steel bearing plates was governed by a surface-to-surface contact pair formulation, using “Hard contact” in the normal direction and a friction coefficient of 0.4 in the tangential directions. The authors performed an initial linear buckling (eigenvalue) analysis to determine the critical buckling loads and shapes, which showed that the buckling shapes were very similar for all profiles and bearing lengths and, for both load configurations, were governed by the

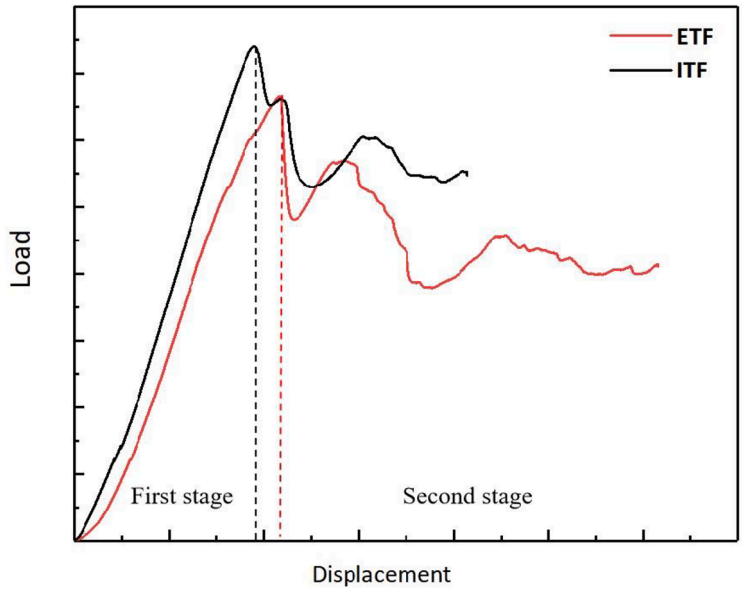


Fig. 6. Typical two-stage load vs. displacement response, which is often observed in web crippling tests in the literature (the figure is used to demonstrate the pattern so the units of load and displacement are not given).

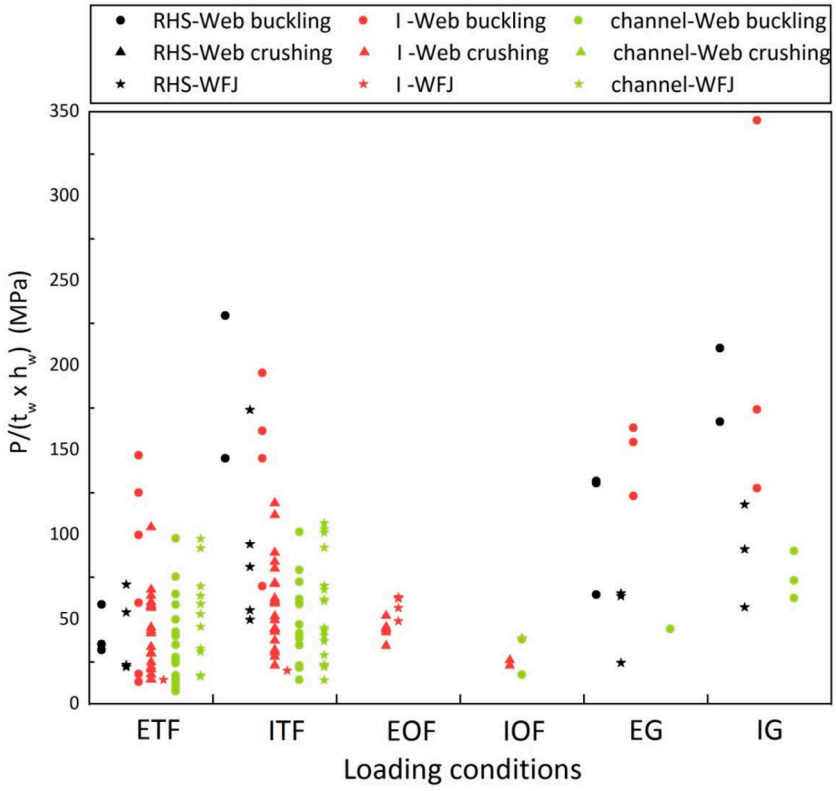


Fig. 7. The effect of section shape on the failure mode and web crippling capacity per unit web area under different loading conditions.

transverse buckling of the webs. On the other hand, the buckling loads increased significantly with the bearing length, particularly for the stockier profiles. Afterwards, the authors performed geometrically non-linear analysis, using the first buckling mode retrieved from the previous analysis as an imperfection, with an amplitude of 1/2000 of the web height. In this analysis, the authors used the Tsai-Hill failure index [39] to estimate the failure initiation on the GFRP laminates (assumed homogeneous across their thickness), using the corresponding strengths derived from the material characterization tests [9]. The results showed that the FE models developed were able to predict the initial shape of the load vs. displacement curves and that the stresses governing the Tsai-Hill failure index were consistent with the experimental failure modes (web-crushing and web-buckling). Conversely, the authors concluded that this failure initiation index is very conservative for strength predictions, underestimating the ultimate loads by 34% to 70%. Therefore, the authors highlighted the need to consider progressive failure models in future numerical research about the web-crippling of FRP profiles.

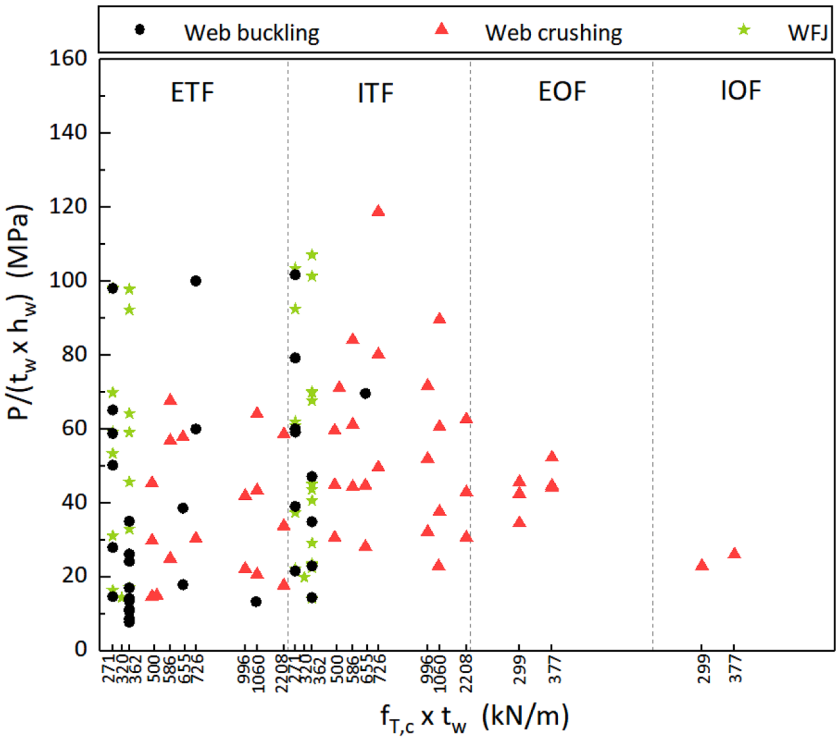


Fig. 8. The effect of web transverse crushing capacity (transverse compressive strength per unit web length) on the failure mode and web crippling capacity per unit web area under different loading conditions.

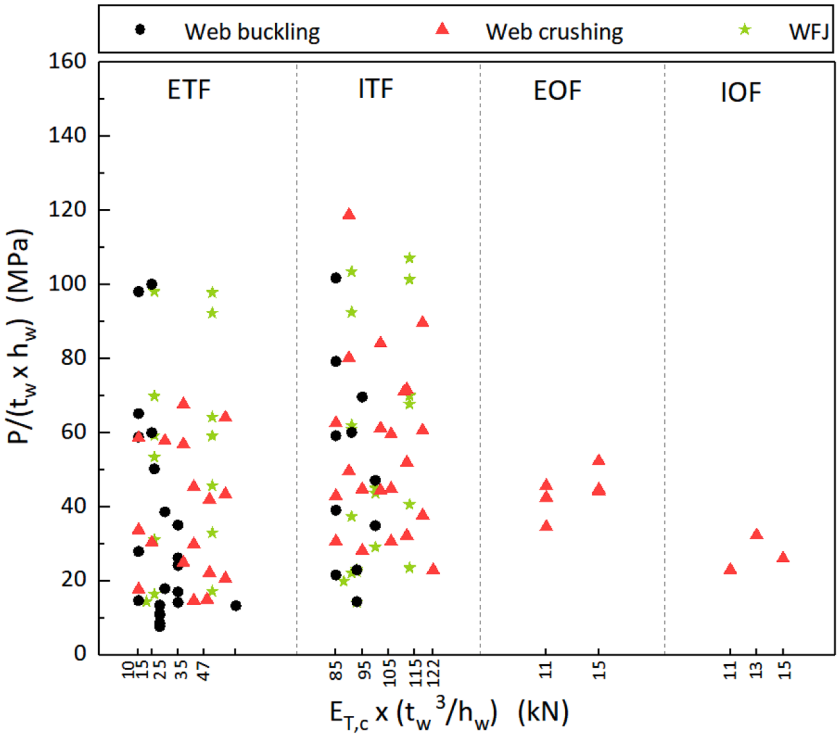


Fig. 9. The effect of web transverse flexural stiffness on the failure mode and web crippling capacity per unit web area under different loading conditions.

Following that recommendation, Nunes et al. [40] modelled part of the same experimental results, namely those of the I-shaped 200 × 100 × 10 mm (I200) profile for ETF and ITF load configurations (ITF/ETF200 [9] *cf.* Table S1). Also using the ABAQUS software package [38], instead of predicting failure with the Tsai-Hill criteria (for which, predictions had ranged from 36% to 41% of experimental failure loads [22]), the authors applied the Hashin failure initiation criteria [32], together with a fracture energy-based damage progression model proposed for composite materials by Camanho and Dávila [41], both built-in the software library [38]. To that end, the main modification to

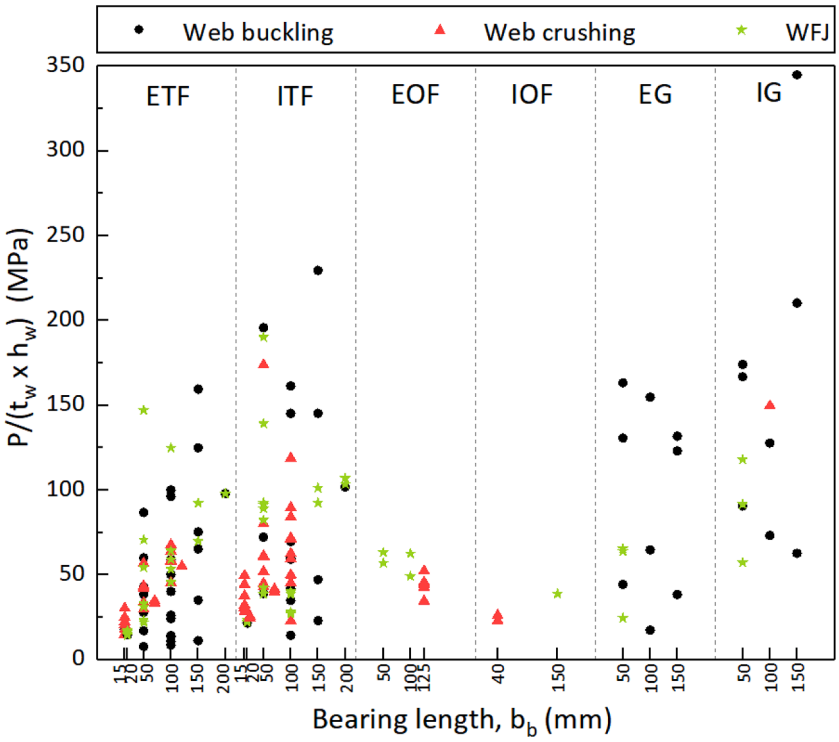


Fig. 10. The effect of bearing length on the failure modes and web crippling capacity per unit web area under different loading conditions.

the previous models was the use of continuum shell elements (SC8R) to model the GFRP laminates, which are 3D elements with 2D kinematic and constitutive behaviour, instead of conventional shell elements. The four fracture energies required as input (longitudinal/transverse – tension/compression) were adopted based on a previous study by the authors [42] on the flexural behaviour of the same I200 profiles. However, the authors highlighted the well-founded uncertainty in the determination of these fracture energies, particularly those concerned with matrix (transverse) failure, which govern web-crippling failure. Based on these assumptions, the authors performed non-linear physical and geometric analysis for the I200 profile, showing that, although the failure load predictions improved significantly in comparison to those performed with the Tsai-Hill failure criterion [22], they were still very conservative, ranging from 59% to 74% with respect to experimental data. In light of these results, and given the uncertainty on some of the input values used, the authors performed parametric analyses, considering the ETF and ITF loading cases with intermediate bearing length (50 mm), changing the following parameters: (i) transverse compressive and (ii) in-plane shear strengths, in a range of −20% to +20% with respect to the experimental values; (iii) matrix compressive fracture energy, ranging from 0.73 to 50 times the initially adopted value [42]; and (iv) the geometry of the web-flange junction, changing it from a sharp corner to a smoother transition made by two slightly wider finite elements. The results showed that, while the in-plane shear strength had a higher influence in the failure initiation load, the ultimate load was more susceptible to variations of the transverse compressive strength, highlighting the importance of both parameters in the web-crippling phenomena. In fact, for the section geometry and load conditions analysed in this study, failure initiation was governed by in-plane shear near the edges of the bearing plate, while the ultimate failure was governed by the transverse compression. Regarding the variation of the matrix compressive fracture energy, the results showed that very large input values (25 and 50 times the reference values) led to simulations in which the failure was not brittle, unlike what had been reported in the experiments. On the other hand, the lower input values (0.73, 1 and 5 times the reference value) considerably underestimated the failure load, with collapse being triggered almost immediately after failure initiation. The authors found out that an input value 10 times higher than the reference value led to a reasonable compromise between the failure nature and the predicted failure load, underestimating the experimental strength by 21% and 23% for the ETF and ITF loading configurations, respectively. These results showed that this fracture energy has a major impact on the quality of the simulation and that the experimental determination of this value is of major importance for the FE modelling of the web-crippling phenomena using fracture energy-based damage progression models. Finally, the consideration of thicker elements to model the web-junction fillet improved the accuracy of the maximum load predictions, with relative differences of −10% and −16% for the ETF and ITF loading configurations, respectively. This showed the importance of correctly modelling the geometry of this specific location.

To address the uncertainty reported by Nunes et al. [40] regarding the input fracture energies, Almeida-Fernandes et al. [33,43,44] developed an experimental study to determine the transverse compressive fracture toughness of several pultruded GFRP materials taken from I- and U-sections produced by different manufacturers. The results of those experiments, in particular the transverse compressive fracture toughness, were used by Almeida-Fernandes et al. [45] as input for the numerical simulation of ITF and ETF web-crippling tests performed on four different I-section profiles and one U-section profile ([23], Table S1). The authors developed FE models similar to those used by Nunes et al. [40] using the ABAQUS software package [37] and applied the Hashin failure initiation criteria [32] together with the built-in fracture energy-based damage progression model [41]. However, unlike the preceding study, the input fracture energies were now determined from independent experimental data [33,43,44]. The authors modelled a simplified geometry, ignoring the web-flange junction fillet, using 4-node shell elements with reduced integration (S4R), and performed geometrical and physical non-linear analyses similar to those reported in [40]. The numerical results compared well with their experimental counterparts, particularly in terms of ultimate load and initial stiffness, with relative differences ranging from −22% to 13% and −17% to 13%, respectively. The authors also reported a good agreement between the

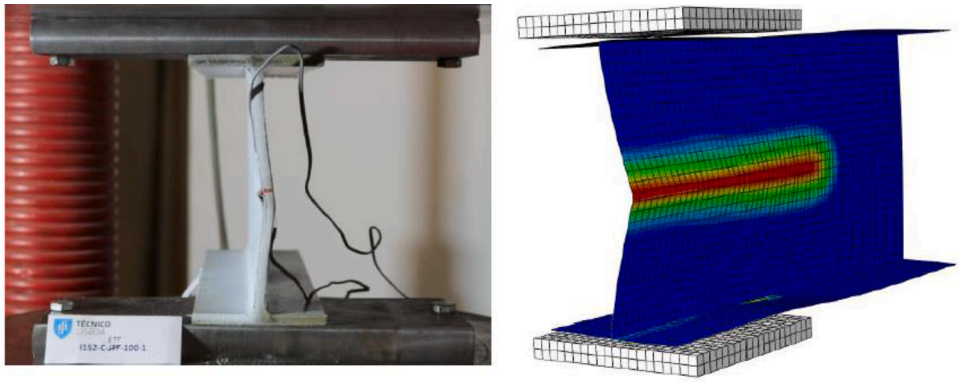


Fig. 11. Comparison between experimental and numerical failure mode [46].

numerical and experimental transverse compressive strain distribution; the numerical shear strain distribution differed significantly from that obtained in the experiments, and this was attributed to the simplifications in the modelling of the web-flange junction. Additionally, the damage modes and damage progression were also well predicted by the FE models, as exemplified in Fig. 11. The authors also highlighted the importance of considering both material and geometrical non-linearities in the modelling of web-crippling phenomena, particularly for profiles with slenderer webs.

The accuracy of a recently proposed damage propagation model [47] was assessed considering experimental web-crippling tests of an I-section 150 × 75 × 8 mm GFRP profile [23] (Table S1) under ITF and ETF loading configurations. For that purpose, Gonilha et al. [34] used the ABAQUS software package [38] and introduced the aforementioned damage propagation model [47] with a user-defined material (UMAT). The GFRP material was modelled as anisotropic, i.e. considering different properties in all directions. Most of the strength and elastic properties of the GFRP laminates (webs and flanges) were retrieved from experimental characterization tests, with the exception of the through-thickness properties, which were taken from the literature. The standardized material characterization tests were also used to calibrate the parameters governing the progressive failure model [47]. The steel bearing plates were modelled with an isotropic linear-elastic material. The specimens were modelled mainly with 8-node solid elements with reduced integration (C3D8R), allowing the use of 6-node wedge elements (C3D6) to model the web-flange junction fillet, which was thus simulated with its nominal radius. To reduce the computational costs, and after a preliminary linear buckling analysis showing that the critical load was approximately twice the experimental strength, symmetry boundary conditions were adopted, resulting in the modelling of a quarter specimen for the ITF loading configuration and an eighth specimen for ETF loading configuration. The models developed were able to predict the web-crippling behaviour for the two loading cases tested (ITF and ETF with bearing lengths of respectively 15 mm and 100 mm). The predicted failure loads underestimated the experimental strengths by −7% to −19%, depending on the mesh, which is a significant improvement in comparison to the previously reported research, showing the feasibility of using that damage progression model to determine the web-crippling strength. The results also showed that for the ITF loading case, failure was triggered by shear stresses, while for the ETF load configuration the transverse compressive stresses governed the failure onset. Additionally, for the first time, the post web-crippling failure behaviour was correctly predicted by FE modelling, with the residual strength prediction being well within the experimental scatter, which is an important aspect for the design of structures with progressive failure modes. Equally important, the models were also well able to predict the damage modes and failure progression patterns observed in the experimental tests, as illustrated in Fig. 12.

Recently, Haloi et al. [48,49] investigated the effects of web perforations on the web-crippling behaviour of GFRP wide-flange profiles, and developed numerical models to simulate their experimental results. The modelling strategies proposed by Nunes et al. [39] were replicated. The authors reported a good agreement regarding the maximum loads and failure modes, but were not able to extend the numerical analysis beyond the peak point. Additionally, the authors used fracture energy values proposed by Nunes et al. [39], which, as mentioned earlier, involve significant uncertainty.

The literature review of the numerical modelling of the web-crippling phenomena in pultruded GFRP profiles shows the evolution of numerical analyses carried out over the last decade. It has shown that while commercially available numerical tools may be able to predict web-crippling failure loads and damage progression, the input data needed to accurately use these tools, in particular, those related with fracture toughness, has to be obtained from extensive (and complex) material experimental tests. Additionally, only one of the previous studies addressing damage modelling considered the actual geometry of the web-flange junction fillet radius. However, (i) it concerned a single GFRP profile, for which geometric non-linearity was not relevant, and (ii) it considered only two bearing lengths, one for each loading condition (ITF and ETF), thus limiting the scope of the findings. Moreover, none of the studies reported above accounted for the mechanical properties of the matrix-rich web-flange junction. Future research in this area should thus focus on the accurate material and geometrical modelling of that particular zone, considering specific input material properties (elastic, strength and fracture), derived from experimental testing, to quantify their influence on the overall web-crippling performance of pultruded profiles, which is a major challenge.

4. Design guidance and analytical models

4.1. Design guidance

The only design guideline that explicitly provides web crippling provisions is the ASCE pre-standard [7], in which the web crippling specifications are included in Chapter 5.4 for flexural design of beams under concentrated forces. The European Technical Specification CEN/TS 19101 [6] also covers web crippling of FRP profiles in Clause 8.3.5, but it does not provide any design formulae and recommends the web crippling resistance to be determined from testing or numerical modelling.

Eq. (1), as proposed by Borowicz and Bank [8], was adopted in the ASCE pre-standard to predict the section capacity due to web-flange junction failure, P_{WFJ}. It is only applicable to the IOF loading condition and to I-shaped sections with height lower than 305 mm. For any section with greater height, the introduction of vertical bearing stiffeners, directly under the load application length, is recommended by the pre-standard to avoid failure at the web-flange junction.

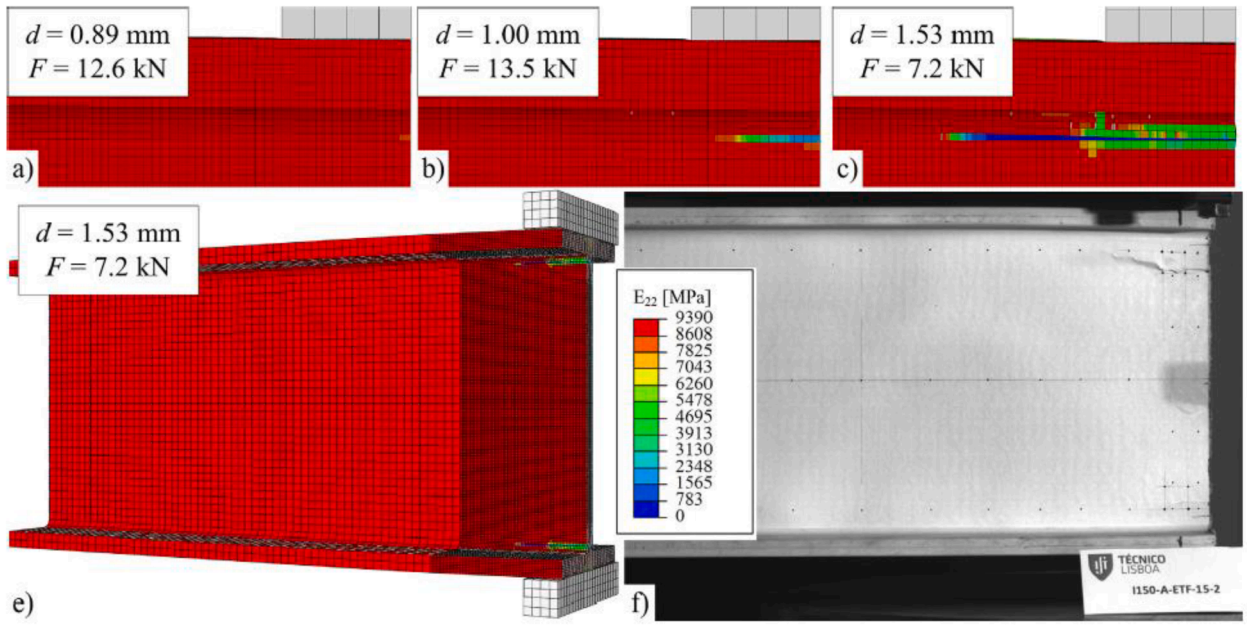


Fig. 12. Damage evolution of the FE model for growing imposed displacements (and corresponding loads) in comparison with experimental failure mode [34].

$$P_{WFJ} = 0.7 H t_w f_s \left[1 + \frac{2k + 6t_b + b_b}{H}\right] \quad (1)$$

where H is the total height of the section, t_w is the web thickness, f_s is the interlaminar shear strength of the web, k is the distance from the top of the flange to the web toe of the fillet, t_b and b_b are the thickness and width of the bearing plate. Most studies normally do not report the thickness of the bearing plate, t_b, which makes it difficult to use this model.

Additionally, the ASCE pre-standard proposes design formula for web buckling capacity under IOF loading condition, P_{WB}, namely by multiplying the critical buckling stress f_{cr} by the effective web area A_{eff}.

$$P_{WB} = f_{cr} A_{eff} \quad (2a)$$

$$f_{cr} = \frac{\pi^2 t_w^2}{6 l_{eff}^2}\left(\sqrt{E_{L,w} E_{T,w}} + E_{T,w}\nu_{LT} + 2G_{LT}\right) \quad (2b)$$

A_{eff} = effective web area = $B_{eff} t_w$

B_{eff} = lesser of the web height and the distance between the vertical web stiffeners

$E_{L,w}$ = (characteristic) longitudinal modulus of the web

$E_{T,w}$ = (characteristic) transverse modulus of the web

G_{LT} = (characteristic) in-plane shear modulus of the web (normally not reported in most studies)

ν_{LT} = (characteristic) longitudinal Poisson's ratio (in absence of available data, $\nu_{LT} = 0.3$)

Eq. (2) is based on the work by Kollár [50], in which it was assumed that the concentrated load is transferred to the web with a load dispersion of 45°, as shown in Fig. 13a and b. Then, the buckling of the web is treated as the buckling of a thin plate with uniformly distributed compression forces and simply supported conditions on the other two edges (Fig. 13c). Eq. (2) does not consider the bearing length, as can be seen from Fig. 13a and from the definition of B_{eff}. Additionally, it should be noted that Eq. (2) is applicable to a section with one web only. For multiple web sections, it should be multiplied by the number of webs.

It must be stressed that the ASCE pre-standard [7] only presented guidance for IOF loading condition, i.e. Eq. (1) for WFJ and Eq. (2) for web buckling failure. However, in Table S7, there are only experimental results for I-shaped sections under IOF loading with WFJ and, as mentioned, most of the results were those from which Eq. (1) was derived. Therefore, it is not possible to assess the performance of the models provided in the ASCE pre-standard. It is recommended that more experimental results are reported in the future. In addition, there is an urgent need to develop suitable design models for other loading conditions considering different failure modes.

4.2. Overview of proposed analytical models

A number of analytical models has been proposed in the literature to predict the web crippling resistance of pultruded FRP profiles. These models are reviewed in this section and their accuracy is assessed against the experimental data presented in Section 2.

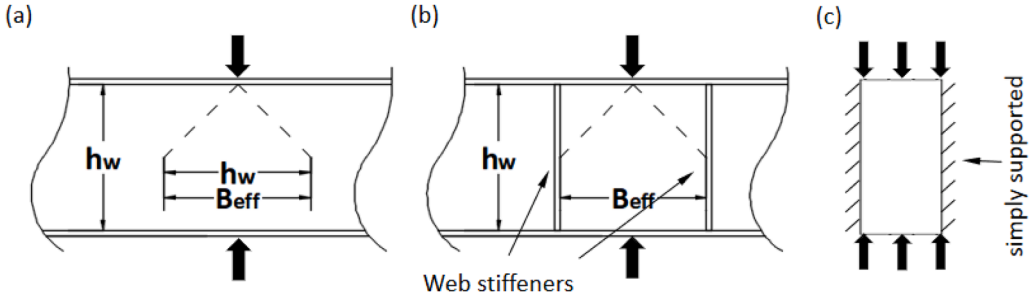


Fig. 13. Load transferring mechanism for web buckling of pultruded GFRP profiles under IOF condition, (a) without or (b) with web-stiffeners, (c) simplified loading model [50].

Wu and Bai [18] proposed an analytical model for pultruded GFRP RHS profiles subjected to ETF, ITF, EG and IG loading conditions. This model only considers the web-flange junction failure with a single shear cracking plane with an inclined angle of 45°, as shown in Fig. 5b. The section resistance (P_{WFJ}), given by Eqs. (3a) to 3b, is defined by the effective area of the shear plane multiplied by f_s. A_{shear} is given by Eq. (3c), where t_w is the web thickness and b_b is the bearing plate length. P_{WFJ} can be determined using Eq. (3a) for ETF and EG, and by Eq. (3b) for ITF and IG.

$$P_{WFJ} = \alpha_e f_s A_{shear} \quad \text{for ETF and EG} \tag{3a}$$

$$P_{WFJ} = \alpha_i f_s A_{shear} \quad \text{for ITF and IG} \tag{3b}$$

$$A_{shear} = 2 \times t_w b_b / cos(45^o) \text{(two webs for RHS)} \tag{3c}$$

α_e and α_i are calibration factors, which were determined using experimental data. For ETF and EG loading, the calibration factor α_e is 0.58, and for ITF and IG loading, α_i is 1.07. It can be seen from Eq. (3) that this model assumes a constant stress distribution at the shear crack plane at the web-flange junction and the length of the crack plane is equal to the length of the bearing plate (b_b).

Wu et al. [10] proposed another analytical model for pultruded GFRP channel sections subjected to ETF and ITF loading conditions. Web-flange junction failure with a shear cracking plane at 45° was also observed for channel sections, as shown in Fig. 5b. Therefore, the section capacity (P_{WFJ}) for web-flange junction failure is given in Eq. (4a). Similar to the RHS, the resistance is defined by the shear plane width multiplied by the integration of the shear stress $f(\tau)$ along the length of the shear plane (B_{eff}). Different from Eq. (3), $f(\tau)$ is not constant along B_{eff}, but is assumed to present a parabolic shape, which was confirmed by means of DIC in the experimental testing. The distribution of $f(\tau)$ is depicted in Fig. 14 and can be calculated with Eq. (4b) for ETF and by Eq. (4c) for ITF.

$$P_{WFJ} = \alpha \frac{t_w}{\sin 45^0} \int f(\tau) dx \tag{4a}$$

$$f(\tau) = -\frac{f_s}{B_{eff}^2} X^2 + f_s \quad \text{for ETF} \tag{4b}$$

$$f(\tau) = -\frac{4f_s}{B_{eff}^2} X^2 + f_s \quad \text{for ITF} \tag{4c}$$

After some rearrangement, P_{WFJ} is given by Eq. (4d), where L is the length of the specimen and B_{eff} is determined with Eq. (4e) for ETF and

Table 3
Dispersion length and effective length of specimens with WFJ failure [10].

Bearing length, b_b (mm)	Dispersion length, a (mm)	Effective length, B_{eff} (mm)	
		ITF	ETF
20	30	80	50
50	50	150	100
100	75	250	175
150	100	350	250
200	110	420	310

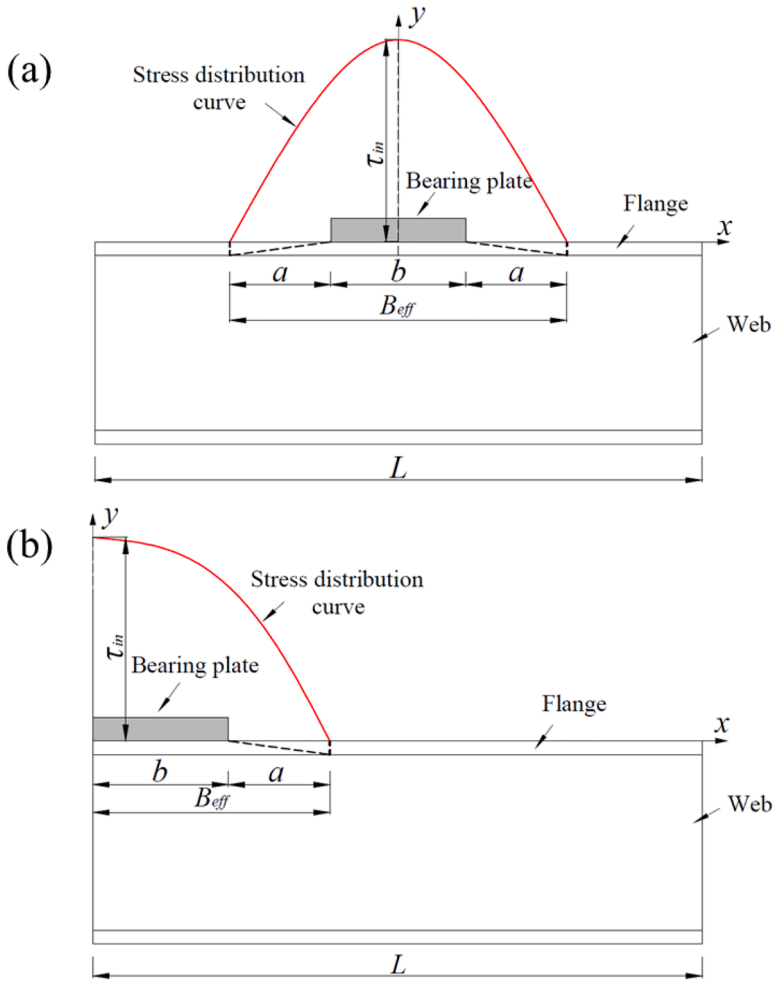


Fig. 14. Load transferring mechanism of specimens with initial web-flange junction failure under (a) ITF and (b) ETF loading conditions [10].

with Eq. (4f) for ITF, where a is the dispersion length of the bearing load from the flange surface to the web-flange junction. This dispersion length a is affected by the bearing length b_b as given in Table 3, which was reported by Wu et al. [10]. The calibration factor, α, was determined from experimental results and it is around 1.0 for ETF and 0.8 for ITF.

$$P_{WFJ} = \alpha \frac{t_w}{\sin 45^0} f_y K \left(1 - \frac{K^2}{3B_{eff}^2}\right) \quad \text{where } K = \min\{B_{eff},\ L\} \tag{4d}$$

$$B_{eff} = b_b + a \ \text{ for ETF} \tag{4e}$$

$$B_{eff} = b_b + 2a \ \text{ for ITF} \tag{4f}$$

Wu et al. [10] stated that the web crippling capacity of a pultruded GFRP profile is given by the minimum of P_{WFJ} and P_{WB}, as expressed in Eq. (4) g. They observed web buckling failure in their tests of channel sections, and proposed a formula to determine the buckling capacity P_{WB}, given by Eq. (4h), which is based on a load transfer mechanism given in AS 4100 [51] for metallic sections. This load transfer mechanism is illustrated in Fig. 15. Based on this model, the web buckling of the channel section is considered equivalent to the buckling of a thin plate whose critical stress, f_{cr}, is given by Eq. (4m). It should be noted that this web buckling model depicted in Fig. 15 is borrowed from that of metallic sections and the actual load transfer mechanism of pultruded GFRP profiles should be determined in future studies.

$$P_n = min\{P_{WFJ},\ P_{WB}\} \tag{4g}$$

$$P_{WB} = \phi f_{cr} A \tag{4h}$$

$$A = Kt_w \tag{4i}$$

$$K = min\{B_{eff},\ L\} \tag{4j}$$

$$B_{eff} = b_b + \frac{H}{2} + 1.5t_w \ \text{for ETF} \tag{4k}$$

$$B_{eff} = b_b + H + 3t_w \ \text{for ITF} \tag{4l}$$

$$f_{cr} = \frac{\pi^2 E_{T,w}}{\lambda_\omega^2} \tag{4m}$$

$$\lambda_\omega = \frac{L_e}{\gamma} = \frac{k_e h_w}{\gamma} \tag{4n}$$

$$h_w = H - 2t_f \tag{4o}$$

$$I = \frac{1}{12} B_{eff} t_w^3 \tag{4p}$$

$$\gamma = \sqrt{\frac{I}{A}} = \frac{t_w}{\sqrt{12}} \tag{4q}$$

$$E = \psi\left(\sqrt{E_{L,w}E_{T,w}} + E_{T,w}\upsilon_{LT} + 2G_{LT}\right) \tag{4r}$$

where ϕ is a modification factor, ϕ=1.055, k_e is the effective length factor, which is taken as 1.0 for sections with web slenderness lower than 100, and as 1.35 for sections with web slenderness greater than 100. ψ is taken as 1/4. Similarly, the shear modulus G_{LT} is not normally reported in most studies.

Chen and Wang reported analytical models for pultruded GFRP RHS [19], I-shaped section [20], and channel section [21] subjected to ETF, ITF, EG and IG loading conditions. These models are presented in Eqs. (5a)-(5c), respectively. These models are obtained through modifications of the design formulae given in Eurocode 3 [52], based on a parametric study for different section dimensions. The k factors associated to these models were calibrated with experimental results and are listed in Table 4. It should be noted that the failure mechanism is not considered in these models. Furthermore, these models may not be applicable when the material properties change, because the calibration of the k factors only considered geometric parameters.

$$P_n = k_1\left(k_2 - \frac{(H-2t_f)/t_w}{k_3}\right)\left(1 + k_4\frac{(b_b-100)^2}{t_w}\right) \ \text{for RHS sections} \tag{5a}$$

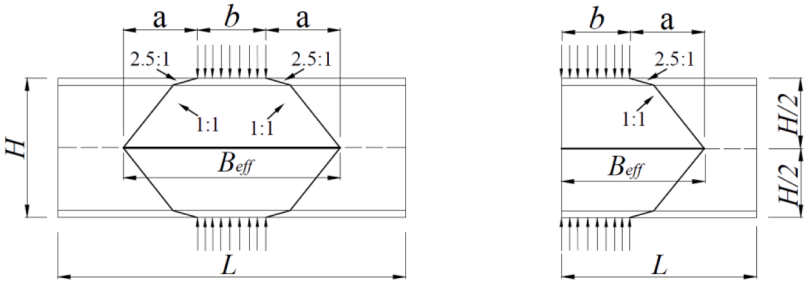
$$P_n = k_1\left(k_2 - \frac{(H-2t_f)/t_w}{k_3}\right)\left(1 + k_4\frac{b_b}{t_w}\right)t_w^2 f_{L,t} \ \text{for } I-\text{shaped sections} \tag{5b}$$

$$P_n = k_1\left(k_2 - \frac{(H-2t_f)/t_w}{k_3}\right)\left(1 + k_4\frac{k_5}{t_w}\right)t_w^2 f_{L,t} \ \text{for channel sections} \tag{5c}$$

However, the authors used the longitudinal tensile strength of the pultruded section $f_{L,t}$ to calculate the web crippling capacity, which is questionable since the load is applied in the transverse direction.

Table 4
Coefficients k_1, k_2, k_3, k_4, k_5 proposed by Chen and Wang [19–21].

Section shape	Loading condition	k_1	k_2	k_3	k_4	k_5
RHS	ETF	0.8	7	60	0.002	NA
	ITF	0.8	16	16	0.0002	
	EGF	0.8	6	130	0.002	
	IGF	0.8	15	50	0.0002	
I-shaped	ETF	1	9	60	0.01	NA
	ITF	1	12	16	0.01	
	EGF	1	9	130	0.01	
	IGF	1	9	50	0.01	
Channel	ETF	1	3	60	0.001	b_b
	ITF	1	4	16	0.001	$(b_b-100)^2$
	EGF	1	1	130	0.004	$(b_b-100)^2$
	IGF	1	6	50	−0.01	b_b



(a) (b)

Fig. 15. Load transfer mechanism of specimens with web buckling failure under (a) ITF and (b) ETF loading conditions [10].

Almeida-Fernandes et al. [22] proposed an analytical model for the web crippling capacity of pultruded I-shaped sections under ITF and ETF loading conditions given below:

$$P_n = Cf_{T,c}h_w^2\left(1 - C_r\sqrt{\frac{r}{t_w}}\right)\left(1 + C_{Lh}\frac{h_w^2}{t_w^3}\right)\left(1 - C_x\frac{h_w}{t_w}(1-\chi_F)\right) \tag{6a}$$

where r is the sum of the radius of the web–flange junction and the thickness of the web (unfortunately the radius of the fillet at the junction is normally not reported in most studies), χ_f is a buckling reduction factor, which can be determined using the following equations:

$$\chi_F = \frac{0.5}{\bar{\lambda}_F} \tag{6b}$$

$$\bar{\lambda}_F = \sqrt{\frac{B_{eff}t_w f_{T,c}}{f_{cr}}} \tag{6c}$$

$$f_{cr} = 0.9k_f E_{T,w}\frac{t_w^3}{h_w} \tag{6d}$$

$$B_{eff} = b_b + 2t_f(1 + \sqrt{m_1 + m_2}) \tag{6e}$$

$$m_1 = \frac{b_f}{t_w} \tag{6f}$$

$$\begin{cases} m_2 = 0.02\left(\frac{h_w}{t_f}\right)^2 \text{ for } \bar{\lambda}_F > 0.5; \\ m_2 = 0 \text{ for } \bar{\lambda}_F < 0.5; \end{cases} \tag{6g}$$

where f_{cr} is the web critical stress and k_f is a coefficient related to the load configuration. It should be noted that the formulae above are empirical and based on the North American Standard (NAS) [53] and Eurocode 3, part 1–5 [52] for metallic sections. C, C_r, C_{Lh}, C_χ are empirical coefficients calibrated with experimental results and they have different values for ETF and ITF loading conditions (see Table 5). The authors also pointed out that these C coefficients may not be applicable to bearing lengths greater than 100 mm. It should be noted that the C factors may be different if used for experimental results from other studies. This is also a limitation of this model.

Table 5
Empirical coefficients calibrated by the experimental results given in [22].

Load condition	C	C_r	C_{Lh}	C_χ
ETF	0.0688	0.5757	0.0037	0.0647
ITF	0.1489	0.5492	0.0015	0.0634

Almeida-Fernandes et al. [46] presented a more recent approach, based on the direct strength method (DSM). The web crippling bearing capacity, P_n, is determined as a function of web crushing capacity, P_{WC}, and web buckling capacity, P_{WB} [54–57].

$$P_n = \begin{cases} P_{WC}, \text{ for } \lambda < 0.776 \\ 1.132P_{WC}\left[1 - 0.280\left(\frac{P_{WB}}{P_{WC}}\right)^{0.930}\right]\left(\frac{P_{WB}}{P_{WC}}\right)^{0.930}, \text{ for } \lambda \geq 0.776 \end{cases} \tag{7a}$$

$$\lambda = \sqrt{\frac{P_{WC}}{P_{WB}}} \tag{7b}$$

$$P_{WB} = k_F\frac{\pi^2 E_{T,w}}{12(1 - \upsilon_{LT}\upsilon_{TL})}\frac{{t_w}^3}{h_w} \tag{7c}$$

$$P_{WC} = B_{eff}t_w f_{T,c} \tag{7d}$$

$$k_f = \begin{cases} \left(5.758 + \frac{b_b}{6.261t_w}\right)\left(0.200 + \frac{b_b}{3.892h_w}\right) \text{ for ETF}; \\ \left(5.014 + \frac{b_b}{8.448t_w}\right)\left(0.611 + \frac{b_b}{7.771h_w}\right) \text{ for ITF}; \end{cases} \tag{7e}$$

$$B_{eff} = \begin{cases} 1.312t_w + 0.918b_b \text{ for ETF}; \\ 2.859t_w + 0.933b_b \text{ for ITF}; \end{cases} \tag{7g}$$

where, k_f is a calibrated buckling coefficient dependent on the loading configuration and geometrical parameters. The orthotropic Poisson's ratios υ_{LT} and υ_{TL} have typical values for pultruded GFRP profiles of 0.3 and 0.1, respectively. B_{eff} was calibrated in [46].

The authors reported that this model could be used to predict failure modes, i.e. web crushing for λ<0.776, web buckling for λ>1.0, and

Table 6
Analytical models in the literature and their conditions of application.

Model ID.	Section shape	Section dimension (mm)*	Bearing length, b_b (mm)	Loading condition	Failure mode*
Eq. (1) and (2)	I-shaped	H: 152 to 304 W: 76 to 304 t_f: NA t_w: 6 to 13	50, 100, 150	IOF, EOF	WFJ
Eq. (3)	RHS	H: 50 and 100 W: 50 and 100 t_f: 4 to 10 t_w: 4 to 10	50	ETF, ITF, EG, IG	WFJ
Eq. (4)	Channel	H: 100, 150, 200 W: 30, 35, 40, 55 t_f: 5, 6.5 t_w: 5, 6.5	20, 50, 100, 150, 200	ETF, ITF	WFJ WB
Eq. (5)	RHS I-shaped Channel	H: 100 W: 50 t_f: 5 t_w: 5	50, 100, 150	ETF, ITF, EG, IG	For RHS and I-shaped: WFJ WB WC For channel: WB
Eq. (6)	I-shaped	H: 92, 114, 190, 385 W: 50, 60, 100, 200 t_w: 6, 8, 10, 15	15, 50, 100	ETF, ITF	WB WC
Eq. (7)	I-shaped	H: 150, 200, 400 W: 70, 100, 150 t_w: 6, 8, 10, 15	15, 50, 100	ETF, ITF	WB WC

* WFJ-web-flange junction failure, WB-web buckling, WC-web crushing.

combined web crushing and web buckling when $0.776 \leq \lambda \leq 1.0$. It was recommended that more accurate monitoring methods should be developed to identify the exact failure mode in a given specimen. It should be noted that this model was developed for I-shaped sections, under ETF and ITF conditions. More experimental data are needed to improve it to address a wider range of sections and loading cases.

Table 6 summarizes the main features of the above-mentioned analytical models, including their conditions of applicability, namely section shape, section dimensions, bearing length, loading conditions and failure modes. It should be noted that only Eqs. (3), (4) and (7) consider the failure modes separately, while the other models do not distinguish different failure modes. In addition, most of the analytical models are applicable to ETF and ITF loading conditions, which are the most investigated in the literature compared with the other loading conditions.

4.3. Comparison between analytical predictions and experimental data

To assess the accuracy of the analytical models presented in the preceding section, the existing experimental data was compared to their analytical predictions of web crippling capacity. These results are presented in Tables S6, S7 and S8 for ETF/ITF, EOF/IOF and EG/IG loading conditions, respectively. The comparisons are also shown in Fig. 16 for ETF/ITF, Fig. 17 for EOF/IOF and Fig. 18 for EG/IG. It should be noted that, when using the analytical models, the criteria for model application is based on loading conditions and availability of material properties. If a model is not applicable for a given loading condition (see Table 6), or if relevant material properties have not been provided (such as the radius of the fillet at the web-flange junction or the web shear modulus), then the predictions with that model are not given. For example, Fig. 16 and Table S6 are for ETF and ITF loading conditions, so Eq. (1) and (2) are not applicable and not used for calculations. The specimens in Tables S6 to S8 are from the literature and they are renamed to highlight the key parameters. The name of specimens consists of three parts, A-B-C, where A is the section shape, B is the loading condition and C is the bearing length.

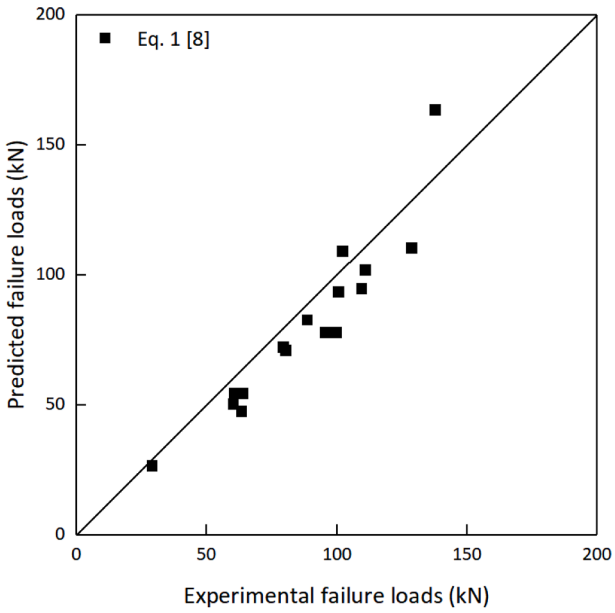


Fig. 17. Comparison between predicted failure loads and experimental results for EOF and IOF loading conditions.

For ETF and ITF loading conditions, from Fig. 16 and Table S6, it is obvious that the analytical models could only accurately predict the experimental results which were used for developing the respective models. However, they all fail to generate accurate predictions of the experimental results reported by other researchers. The predicted web crippling capacities are either much greater or lower than the corresponding experimental results. For example, it seems that Eq. (6) produces relatively accurate predictions with most data points falling on the diagonal line in Fig. 16; however, this is not true, because those data

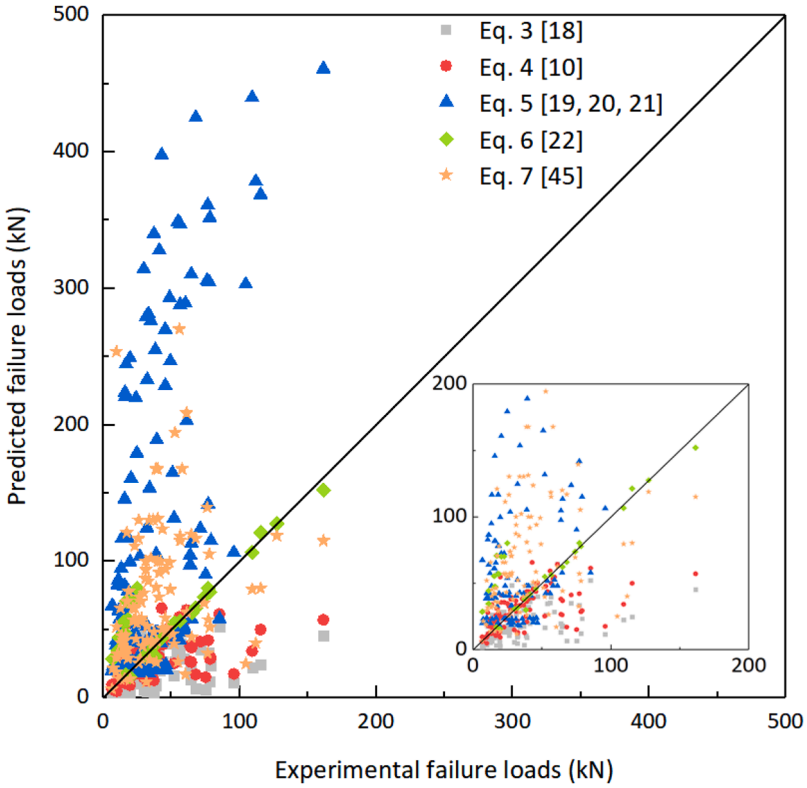


Fig. 16. Comparison between predicted failure loads and experimental results for ETF and ITF loading conditions.

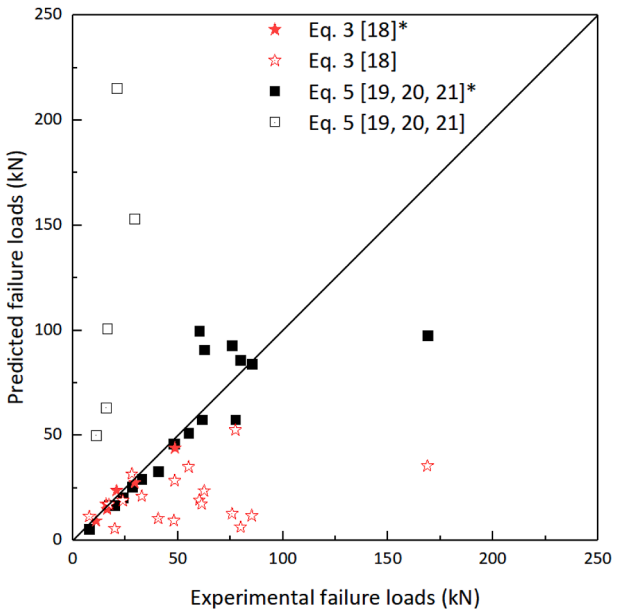


Fig. 18. Comparison between predicted failure loads and experimental results for EG and IG loading conditions (* means the model predictions were compared with the experimental data that were used for developing the respective model).

points on the diagonal line are the predictions of the experimental data which were used for developing Eq. (6). The authors in [24] used this model and reported that the predictions with Eq. (6) were generally greater than the experimental ones (see the off-diagonal points of this model in Fig. 16). In addition, Eq. (6) requires the radius of the fillet at the web-flange junction, which is often not reported in the literature. This is also the reason why Eq. (6) was not applied to other experimental data in Fig. 16.

For EOF and IOF loading conditions, in Fig. 17 and Table S7, Eq. (1) is used for the predictions because other analytical models are not applicable for EOF and IOF conditions. In addition, there are no available experimental data for the web bucking failure mode under EOF and IOF conditions, so Eq. (2) cannot be used. As expected, Eq. (1) is quite accurate with an average bias of 1.12 and a standard deviation of 0.11. This is again because the predictions are compared with the experimental results that were originally used in the derivation of Eq. (1). Therefore, it can be concluded that, although Eqs. (1) and (2) are the only available analytical model in the design specifications, their accuracy has not been confirmed. They should be validated with additional independent experimental results. It should also be noted that Eqs. (1) and (2) require properties like thickness of the bearing plate, elastic modulus and shear modulus of the web in the transverse direction, which should be characterized in future experimental studies in order to assess the accuracy of these models.

For EG and IG loading conditions, in Fig. 18 and Table S8, Eqs. (3) and (5) are considered because they are the only models applicable to these loading conditions. Eq. (3) was developed in [18], while Eq. (5) was developed in [19–21]. It is obvious in Fig. 18 that these models are accurate when they are used to predict the experimental results in the respective references. However, when these models are used for cross validation, i.e. using Eq. (3) to predict results in [19–21] while using Eq. (5) to predict results in [18], that accuracy is lost.

5. Recommendations and outlook

Web crippling used to be a technical term to describe the failure behaviour of thin-walled metallic sections when subjected to transverse concentrated loading. This term is extended to pultruded GFRP profiles just to comply with the traditional terminology in existing international standards for metallic sections, for which web crippling comprises web yielding and web buckling failure modes. However, for pultruded GFRP profiles, web crippling is characterized by a series of new failure mechanisms, including web-flange junction failure, web buckling and web crushing. Furthermore, mixed-modes may occur; for instance, web-flange junction failure may trigger buckling of the webs.

The mechanisms of each of the individual failure modes mentioned above for pultruded GFRP profiles are not yet fully understood. Web buckling mechanism was borrowed from that of metallic sections, so the actual load transfer mechanism should be determined in future studies. Moreover, mixed-mode failure has been reported, increasing the complexity of the web crippling phenomena. The interaction between different failure modes is still unclear, which makes it difficult to associate the peak load with the failure modes. This is also the reason why most analytical solutions do not distinguish different failure modes. Therefore, the development of experimental or numerical techniques is encouraged to distinguish the sequence of the different failure modes in web crippling testing. This is crucial for a better understanding of how the transverse concentrated loading is transferred from the flange(s) to the web(s), so that the failure mechanisms can be fully disclosed.

It is recommended to carefully and comprehensively characterize the geometric and material constitutive models and complex stress state at the web-flange junction where most failure mechanisms initiate in web crippling testing. Currently, there is no study to investigate the effect of the corner radius at the web-flange junction on the web crippling behaviour. The reported results on the effect of bearing length are not fully consistent. The critical material properties, especially the transverse compressive strength and the in-plane and interlaminar shear strengths of the web need to be reported. Also very relevant are the fracture properties, needed as input data in advanced numerical models.

Future numerical studies should also focus on a wider variety of loading conditions, section shapes and section dimensions. Given the complexity of the web crippling failure mechanisms, numerical models can be a powerful tool for design. However, it is essential that future works consider material adapted damage progression models, namely considering the specificities of pultruded materials, and use tri-dimensional formulations, as plane elements may not be able to reproduce the complex stress transfer mechanisms between the flanges and the web. Additionally, it is recommended that future numerical studies use material inputs derived from the mechanical characterization, by experimental testing the particular profiles used, instead of relying on third party data that may not apply.

There is a lack of accurate analytical models and formulae for the web crippling design of pultruded GFRP profiles. Most existing models are developed by fitting experimental results, and heavily rely on the calibration of empirical (calibration) factors. All the other analytical models in Table 6 hardly produce accurate predictions of web crippling capacities when compared with (independent) experimental results. This can be the greatest research gap because web crippling design is impossible without reliable analytical models. On one hand, this lack of precision results from the fact that failure mechanisms are not fully understood, thus empirical approaches become the only option. On the other hand, it is also due to the complex nature of the web crippling behaviour, which is intrinsically three-dimensional and depends on many factors, such as section shapes, section dimensions, material properties, bearing length, loading conditions, etc. Therefore, it is recommended that additional experimental work is conducted, covering a wider range of these key influencing factors. It is encouraged to distinguish different failure modes in the analytical models based on the knowledge of failure mechanisms. This can only be achieved by a combination of comprehensive geometrical and material property characterisations, in-depth understanding of failure mechanisms and occurring sequences, and advancement of numerical modelling technics.

6. Concluding remarks

The web crippling behaviour is very relevant for the design of pultruded GFRP profiles, given their highly orthotropic material properties. Although the research in this topic is recent, it has developed quite fast and provided many important outcomes. This paper reviewed the research advancements in this area and identified critical research gaps that require further development. A database of web crippling experimental data from the relevant literature was developed, which can be used for validation of numerical and analytical models. Recent efforts in numerical modelling techniques to simulate web crippling were reviewed. Guidance for web crippling design was summarized, and analytical formulae to estimate the resistance to web crippling were presented and their accuracy was evaluated against the experimental database. The following main concluding remarks are drawn from the literature review:

(1) Web crippling is a complex failure phenomenon that depends on several geometrical factors, material properties and loading conditions. The geometrical factors include section height, web thickness, flange thickness, radius of the fillet at the web-flange junction, thickness and length of the bearing plate. The material properties include elastic moduli of the web in the longitudinal and transverse directions, compressive strength of the web in the transverse direction, in-plane and interlaminar shear strengths, and fracture energies of both the web and the web-flange junction.
(2) Web crippling failure involves three main mechanisms, not yet fully understood: web-flange junction failure, web crushing and web buckling. The web-flange junction failure is triggered by interlaminar shear stresses at that junction, and this is the most frequently reported failure mode in the literature. The load transfer mechanism associated to web buckling has not yet been fully understood and the interaction between failure mechanisms, namely between web buckling and web crushing, is also another challenge to be addressed.
(3) Numerical models using commercial FE packages are able to simulate with reasonable accuracy the web crippling behaviour of pultruded GFRP profiles, generally providing (sometimes overly) conservative predictions of strength. However, such models require, as input data, an extensive set of elastic, resistance and fracture properties that need to be obtained experimentally. Future efforts should address the influence of material properties and geometry of specific zones of pultruded GFRP profiles, namely the web-flange junctions.
(4) Most analytical models available in the literature do not distinguish failure modes and rely on fitting experimental results. Therefore, they do not provide accurate predictions of web crippling resistance for all design situations, namely different from the ones used for fitting. Additional efforts are thus needed to increase the experimental database and to conduct advanced numerical simulations covering a wider range of parameters. This may help developing more accurate analytical models that finally enable drafting reliable provisions for the web crippling design of pultruded GFRP profiles.

In resume, some critical issues remain unsolved regarding web crippling of pultruded GFRP profiles, and they can be important topics in future research:

(1) Mechanisms of individual failure modes, i.e. web buckling, web crushing and web-flange junction failure, and mode interaction in a mixed-mode failure need to be analysed.
(2) It is important to clarify how the transverse bearing load is transferred from the flange(s) to the web(s), especially for web buckling failure.
(3) The effects of the corner radius and constitutive material model at the resin rich web-flange junction on the web crippling behaviour need to be clarified.
(4) Accurate characterization of the critical fracture energy is needed for accurate numerical modelling.
(5) More phenomenological (less empirical) analytical formulae for design should be developed.
(6) Research on special cases needs to be conducted, including: (i) profiles with holes, (ii) multi-web sections (deck panels), (iii) built-up profiles, (iv) hybrid profiles, (v) effects of elevated temperatures, and (vi) effects of long-term loading.

Declaration of Competing Interest

The authors declare that they have no known competing financial interests or personal relationships that could have appeared to influence the work reported in this paper.

Acknowledgements

The authors acknowledge the support of Fundação para a Ciência e a Tecnologia (FCT) through project PTDC/ECI-EGC/3916/2021 (Reliable-FRP) and the funding of research unit CERIS (UIDB/04625/2020). This work was also supported by FCT, through IDMEC, under LAETA, project UIDB/50022/2020.

Supplementary material

Supplementary material associated with this article can be found, in the online version, at doi:10.1016/j.tws.2023.111128.

References

[1] S.S. Pendhari, T. Kant, Y.M. Desai, Application of polymer composites in civil construction: a general review, Compos. Struct. 84 (2) (2008) 114–124.
[2] S. Russo, A review on buckling collapses of simple and complex columns made from pultruded FRP material, Composites: Mech. Comput. Appl.: Int. J. 8 (1) (2017).
[3] L.C. Hollaway, A review of the present and future utilisation of FRP composites in the civil infrastructure with reference to their important in-service properties, Constr. Build. Mater. 24 (12) (2010) 2419–2445.
[4] J. Wood, Structural design of polymer composites Eurocomp design code and handbook, Edited by John L. Clarke E & FN Spon, London, UK, ISBN 0 419 19450 9, Compos. Struct. 4 (35) (1996) 445.
[5] National Research Council, Guide for the design and construction of structures made of FRP pultruded elements, CNR-DT 205 (2007) 25–31.
[6] CEN/TS 19101, Design of Fiber-Polymer Composite Structures, CEN/TC 250, European Committee for Standardization, Brussels, 2022.
[7] American Composites Manufactures Association, Pre-standard for Load & Resistance Factor Design (LRFD) of Pultruded Fiber Reinforced Polymer (FRP) Structures, ACMA, Arlington, VA, 2012, p. 14.
[8] D.T. Borowicz, L.C. Bank, Behavior of pultruded fiber-reinforced polymer beams subjected to concentrated loads in the plane of the web, J. Compos. Constr. 15 (2) (2011) 229–238.
[9] L.A. Fernandes, J. Gonilha, J.R. Correia, N. Silvestre, F. Nunes, Web-crippling of GFRP pultruded profiles. Part 1: experimental study, Compos. Struct., 120 (2015) 565–577.
[10] C. Wu, L.T. Zhang, Y. Bai, X.L. Zhao, Web crippling behavior of pultruded GFRP channel sections under transverse bearing load, Compos. Struct. 209 (2019) 129–142.
[11] J.A. Packer, Web crippling of rectangular hollow sections, J. Struct. Eng. 110 (10) (1984) 2357–2373.
[12] X.L. Zhao, G.J. Hancock, Square and rectangular hollow sections subject to combined actions, J. Struct. Eng. 118 (3) (1992) 648–667.
[13] B. Young, G.J. Hancock, Design of cold-formed channels subjected to web crippling, J. Struct. Eng. 127 (10) (2001) 1137–1144.
[14] Winter, G., & Pian, R.H.J. Crushing strength of thin steel webs. Engineering experiment station. Bulletin, (35 Part 1).
[15] F. Zhou, B. Young, Aluminum tubular sections subjected to web crippling—Part I:: tests and finite element analysis, Thin Walled Struct. 46 (4) (2008) 339–351.
[16] B. Young, F. Zhou, Aluminum tubular sections subjected to web crippling—Part II: proposed design equations, Thin Walled Struct. 46 (4) (2008) 352–361.
[17] H. Alsanat, S. Gunalan, K. Poologanathan, H. Guan, Web crippling investigations of aluminium lipped channel sections under one-flange loading conditions, Thin Walled Struct. 166 (2021), 108025.

[18] C. Wu, Y. Bai, Web crippling behaviour of pultruded glass fibre reinforced polymer sections, Compos. Struct. 108 (2014) 789–800.
[19] Y. Chen, C. Wang, Web crippling behavior of pultruded GFRP rectangular hollow sections, Composites Part B: Engi. 77 (2015) 112–121.
[20] C. Wang, Test on pultruded GFRP I-section under web crippling, Composites Part B: Eng. 77 (2015) 27–37.
[21] W. Zhang, Y. Chen, Tests on GFRP pultruded profiles with channel section subjected to web crippling, Appl. Compos. Mater. 24 (2017) 849–862.
[22] L.A. Fernandes, F. Nunes, N. Silvestre, J.R. Correia, J. Gonilha, Web-crippling of GFRP pultruded profiles. Part 2: numerical analysis and design, Compos. Struct. 120 (2015) 578–590.
[23] L. Almeida-Fernandes, J.R. Correia, N. Silvestre, Effect of fibre layup and bearing length on the web-crippling behaviour of pultruded GFRP profiles, Compos. Struct. 267 (2021), 113884.
[24] J. Haloi, S.K. Mushahary, A.C. Borsaikia, K.D. Singh, Experimental investigation on the web crippling behaviour of pultruded GFRP wide-flange sections subjected to two-flange loading conditions, Compos. Struct. 259 (2021), 113469.
[25] D.D. Estep, H.V. GangaRao, D.B. Dittenber, M.A. Qureshi, Response of pultruded glass composite box beams under bending and shear, Compos. Part B: Eng. 88 (2016) 150–161.
[26] A.V. Oskouei, M. Bazli, H. Ashrafi, M. Imani, Flexural and web crippling properties of GFRP pultruded profiles subjected to wetting and drying cycles in different sea water conditions, Polym. Test. 69 (2018) 417–430.
[27] A. Gand, M. Mohammed, S. Jarrouj, Performance of perforated FRP stub beams subject to static transverse actions, Eng. Solid Mech. 8 (2) (2020) 105–118.
[28] S.B. Singh, H. Chawla, Stability and failure characterization of fiber reinforced pultruded beams with different stiffening elements, Part I: experimental investigation, Thin Walled Struct. 141 (2019) 593–605.
[29] L.T. Zhang, C. Wu, Experimental study on the web crippling behaviour of pultruded GFRP channel sections using DIC, in: MATEC Web of Conferences, EDP Sciences, 2019, p. 01009. Vol. 275.
[30] C. Wu, L.T. Zhang, L.H. Tam, L. Yan, L. He, Effect of bearing length on web crippling behavior of pultruded GFRP channel section, Compos. Struct. 253 (2020), 112810.
[31] T. Nguyen, T.M. Chan, T.J. Mottram, Reliable in-plane shear modulus for pultruded- fibre-reinforced polymer sections, Proc. Inst. Civil Eng. - Struct. Build. 2018 171 (11) (2018) 818–829.
[32] Z. Hashin, Fatigue Failure Criteria for Unidirectional Fiber Composites, Pennsylvania Univ Philadelphia Dept of Materials Science and Engineering, 1980.
[33] L. Almeida-Fernandes, N. Silvestre, J.R. Correia, M. Arruda, Compressive transverse fracture behaviour of pultruded GFRP materials: experimental study and numerical calibration, Compos. Struct. 247 (2020), 112453.
[34] J.A. Gonilha, N. Silvestre, J.R. Correia, V. Tita, L. Almeida-Fernandes, Novel progressive failure model for quasi-orthotropic pultruded FRP structures: application to compact tension and web-crippling case studies (Part II), Compos. Struct. 255 (2021), 112973.
[35] A. Fascetti, L. Feo, N. Nisticò, R. Penna, Web-flange behavior of pultruded GFRP I-beams: a lattice model for the interpretation of experimental results, Composites Part B: Eng. 100 (2016) 257–269.
[36] T. Liu, J.Q. Yang, P. Feng, K.A. Harries, Determining rotational stiffness of flange-web junction of pultruded GFRP I-sections, Compos. Struct. 236 (2020), 111843.
[37] ANSYS 11.0, [Computer Software], Ansys Inc., Canonsburg, PA, 2006.
[38] ASTM. Standard test method for compressive properties of polymer matrix composite materials using a combined loading compression (CLC). American Society for Testing and Materials (ASTM), West Conshohocken. PA. USA (2013) ASTM D6641/D 6641M – 09.
[39] R.M. Jones, Mechanics of Composite Materials, CRC Press, 2018.
[40] F. Nunes, N. Silvestre, J.R. Correia, Progressive damage analysis of web crippling of GFRP pultruded I-sections, J. Compos. Constr. 21 (3) (2017), 04016104.
[41] P.P. Camanho, G.C. Dávila, Mixed-mode decohesion finite elements for the simulation of delamination in composite materials, NAS 1 (15) (2002) 211737.
[42] F. Nunes, J.R. Correia, N. Silvestre, Structural behavior of hybrid FRP pultruded beams: experimental, numerical and analytical studies, Thin Walled Struct. 106 (2016) 201–217.
[43] L. Almeida-Fernandes, N. Silvestre, J.R. Correia, Characterization of transverse fracture properties of pultruded GFRP material in tension, Composites Part B: Eng. 175 (2019), 107095.
[44] L. Almeida-Fernandes, J.R. Correia, N. Silvestre, Transverse fracture behavior of pultruded GFRP materials in tension: effect of fiber layup, J. Compos. Constr. 24 (4) (2020), 04020019.
[45] L. Almeida-Fernandes, N. Silvestre, J.R. Correia, Fracture toughness-based models for web-crippling of pultruded GFRP profiles, Composites Part B: Eng. 230 (2022), 109541.
[46] L. Almeida-Fernandes, N. Silvestre, J.R. Correia, Direct strength method for web-crippling design of pultruded GFRP beams, J. Compos. Constr. 25 (4) (2021), 04021031.
[47] J.A. Gonilha, N. Silvestre, J.R. Correia, V. Tita, D. Martins, Novel progressive failure model for quasi-orthotropic pultruded FRP structures: formulation and calibration of parameters (Part I), Compos. Struct. 255 (2021), 112974.
[48] J. Haloi, A.C. Borsaikia, K.D. Singh, Web crippling behaviour of web perforated GFRP wide-flange sections subjected to interior-two-flange loading condition, Thin Walled Struct. 166 (2021), 108072.
[49] J. Haloi, K.D. Singh, A.C. Borsaikia, Effect of web perforation on the performance of pultruded GFRP wide-flange section profile in web crippling under end-two-flange loading configuration, Thin Walled Struct. 175 (2022), 109187.
[50] L.P. Kollar, G.S. Springer, Mechanics of Composite Structures, Cambridge University Press, 2003.
[51] AS 4100-1998, Steel Structures. Australian Standard AS 4100-1998, Standards Association of Australia, Sydney, Australia, 1998.
[52] EN 1993-1-5, Eurocode 3 - Design of steel structures - Part 1-5: Plated structural elements, CEN/TC 250, European Committee for Standardization, Brussels, 2018.
[53] American Iron and Steel Institute, North American specification for the design of cold-formed steel structural members, in: American Iron & Steel Institute, Committee of Steel Plate Producers & Committee of Stainless Steel Producers, 2007.
[54] Schafer BenjaminW., Pekoz Teoman. Direct strength prediction of cold-formed steel members using numerical elastic buckling solutions, CCFSS Proceedings of International Specialty Conference on Cold-Formed Steel Structures (1971-2018) 4 (1998).
[55] B.W. Schafer, Advances in the Direct Strength Method of cold-formed steel design, Thin Walled Struct. 140 (2019) 533–541.
[56] P. Natário, N. Silvestre, D. Camotim, Direct strength prediction of web crippling failure of beams under ETF loading, Thin Walled Struct. 98 (2016) 360–374.
[57] P. Natário, N. Silvestre, D. Camotim, Web crippling of beams under ITF loading: a novel DSM-based design approach, J. Constr. Steel Res. 128 (2017) 812–824.